



**HAL**  
open science

## Chromatin remodelling by INO80 at promoter proximal pause sites promotes premature termination of mRNA synthesis

Sara Luzzi, Ugo Szachnowski, Sarah Greener, Kenny Schumacher, Stuart Fulton, Camille Gautier, Kang Hoo Han, Jack Darke, Rossana Piccinno, Anne Lafon, et al.

### ► To cite this version:

Sara Luzzi, Ugo Szachnowski, Sarah Greener, Kenny Schumacher, Stuart Fulton, et al.. Chromatin remodelling by INO80 at promoter proximal pause sites promotes premature termination of mRNA synthesis. 2021. hal-03430529

**HAL Id: hal-03430529**

**<https://hal.science/hal-03430529>**

Preprint submitted on 16 Nov 2021

**HAL** is a multi-disciplinary open access archive for the deposit and dissemination of scientific research documents, whether they are published or not. The documents may come from teaching and research institutions in France or abroad, or from public or private research centers.

L'archive ouverte pluridisciplinaire **HAL**, est destinée au dépôt et à la diffusion de documents scientifiques de niveau recherche, publiés ou non, émanant des établissements d'enseignement et de recherche français ou étrangers, des laboratoires publics ou privés.



24 <sup>10</sup>Department of Molecular Biology and Genetics, Cornell University, Ithaca, NY 14853,

25 USA

26 <sup>11</sup>Lead Contact

27 \*These authors contributed equally to this work

28 †Correspondence to: [antonin.morillon@curie.fr](mailto:antonin.morillon@curie.fr) and [manolis.papamichos@newcastle.ac.uk](mailto:manolis.papamichos@newcastle.ac.uk)

29 **Abstract**

30 How co-transcriptional RNA quality control is regulated remains poorly understood. Here,  
31 we report that in *S. cerevisiae* premature transcription termination of mRNAs is regulated by  
32 the evolutionarily conserved ATP-dependent chromatin remodeling INO80 complex. Loss of  
33 INO80 leads to an increase in promoter-proximally paused RNA Polymerase II and defective  
34 progression into the gene body. We show that promoter-proximal transcriptional pausing  
35 correlates with loading of RNA surveillance and transcription termination factors to mRNA  
36 transcripts. Cells lacking INO80 are defective for the Nrd1-Nab3-Sen1 (NNS)-dependent  
37 pathway for transcription termination at snRNA genes and promoter-proximally sites of  
38 mRNA genes. We demonstrate that INO80 promotes the association of the RNA surveillance  
39 and termination factor Nab2 with short promoter-proximal mRNA transcripts. We provide  
40 evidence that co-transcriptional recruitment of Nab2 to chromatin is regulated by INO80,  
41 which enables the interaction of Nab2 with the histone variant H2A.Z. Our work suggests a  
42 chromatin mechanism for premature transcription termination at promoter-proximally  
43 pausing sites, linking RNA quality control to the transcriptional process.

## 44 INTRODUCTION

45 Elimination of aberrant mRNAs is essential for proper gene expression. In eukaryotic cells  
46 nuclear RNA surveillance and quality control mechanisms monitor mRNA biogenesis co-  
47 transcriptionally and terminate transcription prematurely for degradation of the nascent RNA  
48 transcript<sup>1</sup>. Elegant genome-wide studies in the budding yeast *Saccharomyces cerevisiae*  
49 have suggested that unproductive transcriptional elongation of protein coding genes is wide-  
50 spread and common<sup>2,3</sup>. Furthermore, promoter-proximal short mRNAs enriched in 3'-  
51 oligo(A) tails have been identified<sup>4</sup>, indicating extensive premature termination across the  
52 yeast protein-coding genome<sup>5</sup>. Likewise, only 10% of promoter-proximally paused  
53 polymerases was shown to enter productive elongation in human cells, with the remaining  
54 being prematurely terminated during abortive elongation<sup>6,7</sup>.

55 The major nuclear RNA quality control pathway in yeast is mediated by the RNA  
56 surveillance complex Nrd1-Nab3-Sen1 (NNS)<sup>8</sup> and the Rrp6-dependent nuclear exosome  
57 complex with 3' exonuclease activity<sup>9</sup>. The NNS-dependent nuclear RNA quality control  
58 pathway acts prominently to restrict the extensive and pervasive transcription of non-coding  
59 RNAs (ncRNAs)<sup>10</sup>. Nrd1 and Nab3 have also been found to be recruited at active protein-  
60 coding genes with a preference near their 5' end and bind most mRNA transcripts<sup>11-15</sup>,  
61 suggesting a genome-wide role for NNS in mRNA transcription termination<sup>15</sup> and co-  
62 transcriptional control of mRNA metabolism. However, this model has been challenged by a  
63 separate study, which proposed that only a few mRNA genes are subject to transcriptional  
64 attenuation by the NNS complex<sup>16</sup>. Thus, although the RNA surveillance and termination  
65 pathways have been characterized in molecular detail, the mechanisms regulating premature  
66 transcription termination during mRNA synthesis by Pol II remain unclear.

67 In metazoans, short, promoter-associated polyadenylated mRNA transcripts<sup>17</sup> have been  
68 found to associate with Pol II pausing<sup>18</sup>, with premature termination and exosome-dependent

69 degradation coinciding with promoter-proximal pausing sites<sup>19</sup>. Experiments with chemical  
70 transcriptional inhibitors indicated high rates of turnover and premature termination of  
71 promoter-proximal paused Pol II<sup>6,20,21</sup>, suggesting regulation of gene expression by  
72 transcriptional attenuation. Even though promoter-proximal pausing plays an important  
73 regulatory role in eukaryotic transcription<sup>22-25</sup>, how pausing is linked to premature  
74 termination remains poorly understood.

75 Eukaryotic transcription is controlled by the underlying chromatin structure. ATP-dependent  
76 chromatin remodelling enzymes shape the chromatin landscape and act at almost all stages of  
77 RNA production controlling transcription activation and silencing, modulation of  
78 transcriptional rates, transcription termination and RNA export from the nucleus<sup>26-30</sup>. In  
79 mammals, premature termination of mRNA genes and promoter-proximal transcriptional  
80 pausing have been associated with nucleosome organization<sup>19</sup>. However, the role of  
81 chromatin remodelers in co-transcriptional RNA quality control remains elusive.

82 The multisubunit ATP-dependent chromatin remodelling complex INO80 has a well-  
83 established and important role in transcription across eukaryotes<sup>31</sup>. INO80 is enriched at the  
84 transcription start sites (TSS) of most active and poised mRNA genes in yeast and  
85 mammals<sup>32,33</sup>. The nucleosome remodelling activity of INO80 is important for the exchange  
86 of the histone variant H2A.Z for H2A in nucleosomes and for controlling nucleosome  
87 positions<sup>31</sup>. While it is generally proposed that the function of INO80 during transcription is  
88 to control transcription initiation, INO80 physically interacts with the elongating RNA  
89 Polymerase II machinery<sup>34,35</sup> and binds to mRNAs<sup>36,37</sup>. This indicates a -yet- undefined role  
90 for INO80 in the transcriptional process.

91 Here we investigate the role of INO80 in transcription regulation in *S. cerevisiae*. Using  
92 Native Elongating Transcript sequencing (NET-seq) we analyse how the process of  
93 transcription is regulated by INO80 at nucleotide resolution. We show that INO80 enables

94 the progression of Pol II from the promoter-proximal region into the gene body. Our analysis  
95 indicates that promoter-proximal pausing of Pol II is linked to loading of transcription  
96 termination and RNA processing factors to mRNA transcripts. Mechanistically our study  
97 reveals that INO80 modulates the interaction between the RNA surveillance and termination  
98 factor Nab2 and H2A.Z, enabling recruitment of Nab2 to chromatin. Overall, our results  
99 suggest that the chromatin remodelling function of INO80 promotes premature transcription  
100 termination.

101 **RESULTS**

102 **Defective progression of Pol II from the promoter proximal region into the gene body in**  
103 **the absence of INO80**

104 To illuminate the role of INO80 in transcription, we performed Native Elongating Transcript  
105 NET-seq analysis in Wild-Type (WT) and *ino80Δ* yeast cells expressing a FLAG-tag version  
106 of the largest subunit of the RNA Polymerase II complex, Rpb1 (Extended Data Fig. 1a, b).  
107 NET-seq captures nascent RNAs bound to transcriptionally engaged Pol II and sequences the  
108 3'-end of the purified RNAs, thus providing a detailed map of elongating Pol II across the  
109 genome at nucleotide resolution<sup>38</sup>. Therefore, and to avoid confusion with the term “nascent  
110 RNAs” that is commonly used to describe newly synthesized RNAs that are not necessarily  
111 associated with Pol II<sup>39</sup>, we will henceforth refer to the Pol II-associated transcripts captured  
112 by NET-seq as Pol II density.

113 Following removal of duplicated reads and DEseq normalization, NET-seq densities were  
114 computed as normalized counts over gene length and their distribution across the gene was  
115 compared between the two strains. Consistent with previous reports<sup>38,40</sup>, promoter-proximal  
116 region showed sense Pol II density, with a subsequent reduction further into the gene body in  
117 WT cells (Fig. 1a). Interestingly, in *ino80Δ* cells, while sense Pol II density was reduced at  
118 the promoter-proximal peak, it decreased further downstream the promoter-proximal region,  
119 compared to WT (Fig 1a). Changes in the abundance of sense and antisense NET-seq reads at  
120 mRNA genes in *ino80Δ* did not correlate (Extended Data Fig. 1c,  $r=0.04$ ), indicating that  
121 altered sense Pol II density in the absence of INO80 is independent of antisense transcription.

122 We explored whether the decrease in Pol II density downstream the promoter proximal  
123 region in *ino80Δ* indicates defective progression of RNA Polymerase II into the gene body.  
124 To test this possibility, we calculated Traveling Ratio (TR) values for all mRNA genes by

125 comparing the Pol II density in the gene body relative to the promoter-proximal region of the  
126 first 200bp after the TSS (Fig. 1b). In WT cells, 68% of protein-coding genes exhibited  
127 higher Pol II density at the promoter-proximal region compared to Pol II density in the gene  
128 body for (TR<1), indicating accumulation of Pol II proximally to promoter for most of the  
129 genes. Loss of INO80 led to an overall significant reduction in TR, with 809 genes exhibiting  
130 a decrease in TR of at least 1.5 fold-change compared to WT (Fig. 1b). Overall, 73% of genes  
131 demonstrated a TR<1 in *ino80Δ*. This indicates a genome-wide defect in progression of Pol II  
132 from the promoter-proximal region into the gene body in the absence of INO80.

133 INO80 physically interacts with the elongating RNA Polymerase II complex<sup>34,35</sup> and is  
134 enriched within gene bodies<sup>33,41</sup>. To evaluate its role during transcription elongation, we  
135 asked whether the enrichment of INO80 inside gene bodies correlates with the intragenic  
136 levels of Pol II. ChIP-exo analysis provides near single-nucleotide resolution of factor  
137 binding to DNA<sup>42</sup> and can distinguish between recruitment inside and outside the gene body  
138 with great accuracy. When the Ino80<sup>41</sup> and Rpb1 ChIP-exo densities within the gene bodies  
139 were compared, a strong, positive correlation between their enrichment was observed (Fig.  
140 1c, r=0.68). This indicates that the presence of INO80 inside the gene is associated with  
141 transcription elongation activity.

142 Chromatin remodelling activity and functionality of the INO80 complex relies on the INO80-  
143 specific subunits Arp5 and Arp8<sup>31</sup>. Cells lacking either *INO80* or the INO80-specific subunits  
144 *ARP5* or *ARP8* grew poorly in the presence of 6-azauracil (6-AU) (Fig. 1d and Extended  
145 Data Fig. 1d, e), an inhibitor of GTP biosynthesis which sensitizes transcriptional elongation  
146 mutants<sup>43</sup>. Therefore, these results suggest that INO80 promotes transcription elongation,  
147 supporting a genome-wide, post-initiation role for INO80 in gene expression.

148 **Global downregulation of Pol II transcription in the absence of INO80 is associated**  
149 **with defective mRNA degradation**

150 Increase in transcription initiation can lead to enhanced pausing of Pol II at predetermined  
151 sites<sup>44</sup>. We therefore asked whether transcription rates are increased in the absence of INO80,  
152 by comparing the levels of newly synthesized mRNAs in WT and *ino80Δ* cells. Cells grown  
153 in rich medium were pulse-labelled with 4-thiouracil (4tU) and mixed in a fixed ratio with  
154 labelled *S.pombe* cells (spike-in) for normalization<sup>45</sup>. In parallel, 4tU labelling was also  
155 conducted in *ino80Δ* cells expressing wild-type *INO80* from a plasmid, serving as a control  
156 for *ino80Δ*-mediated changes in RNA expression. Purified total (steady state) and labelled  
157 (newly synthesized) RNA from all samples were subjected to sequencing.

158 After normalization to the *S. pombe* spiked-in signal and applying a cutoff of 1.5-fold change  
159 and p-value < 0.05, only 3.6% of all protein coding genes showed significant increase in  
160 newly synthesized mRNA levels in *ino80Δ* (n=178, Fig. 3a). Contrary, 34% of the protein-  
161 coding genome demonstrated a significant reduction in mRNA synthesis in *ino80Δ* compared  
162 to WT (n=1706, Fig. 3a). The downregulation of mRNA synthesis rates was INO80-  
163 dependent, since in *ino80Δ* cells expressing *INO80* from an episomal plasmid, less than 4%  
164 of genes had markedly decreased newly synthesized mRNA levels (n=193, Extended Data  
165 Fig. 3a). Therefore, deletion of INO80 induces genome-wide downregulation of mRNA  
166 synthesis rates, arguing against increased transcription initiation as the underlying cause of  
167 enhanced Pol II pausing in *ino80Δ*.

168 Interestingly, despite the global decrease in newly synthesized mRNA levels in *ino80Δ*, the  
169 cellular, total mRNA levels for 81% of the protein-coding genes did not significantly change,  
170 while 13% were increased in the absence of INO80 (Fig. 3b). This disentanglement between  
171 newly synthesized and total RNAs suggests buffering of mRNA transcript levels<sup>46</sup> in *ino80Δ*  
172 by a compensatory mechanism. Cellular mRNA levels are determined by the rates of mRNA  
173 synthesis and degradation. To understand why cellular mRNA levels remain high in *ino80Δ*,  
174 we conducted comparative dynamic transcriptome analysis (cDTA)<sup>47</sup>, which measures

175 mRNA synthesis and decay rates (SR and DR respectively) for all protein-coding genes.  
176 Comparison of the SR and DR changes in *ino80Δ* relative to WT revealed that the decrease in  
177 SR observed in *ino80Δ* positively correlated with a concomitant decrease in DR ( $r=0.47$ ,  $p$ -  
178 value= $2.9e^{-233}$ , Fig 3c). This indicates that the defect in Pol II transcription in *ino80Δ* is  
179 associated with compromised mRNA degradation, in a similar fashion to what has been  
180 observed for the *rpb1-N488D* mutant<sup>47</sup>, which reduces the processivity of Pol II<sup>48</sup>.

181 To verify that mRNAs are stabilized in the absence of INO80, we analysed mRNA decay  
182 rates following transcription inhibition with thiolutin in WT and *ino80Δ* cells. Thiolutin was  
183 used at concentration below the threshold reported to affect mRNA half-life<sup>49</sup> and mRNA  
184 values were normalized relative to the stable *scR1* RNA, which is transcribed by Pol III. The  
185 relative abundance of *NRD1*, *RNAI* and *HPT1* transcripts, which showed decreased DR in the  
186 cDTA analysis (Extended data Fig. 3b), was markedly higher in *ino80Δ* compared to WT  
187 after transcription inhibition (Fig. 3d and Extended data Fig. 3c). Therefore, the concomitant  
188 change in mRNA synthesis and degradation in *ino80Δ* suggest that the transcriptional role of  
189 INO80 is linked to RNA decay by buffering steady state mRNA levels.

### 190 **Promoter-proximal Pol II pausing is linked to increased loading of RNA surveillance** 191 **and termination factors to mRNA transcripts**

192 The results from our NET-seq and 4tU-seq analysis prompted us to evaluate whether  
193 promoter-proximal pausing is linked to nuclear RNA quality control and premature  
194 transcription termination.

195 The nuclear RNA cleavage and termination factor Nab2<sup>50</sup> and the Trf4/Trf5-Air1/Air2-Mtr4  
196 polyadenylation (TRAMP) complex are required for processing and delivering nascent  
197 transcripts to the nuclear exosome for degradation<sup>51-55</sup>. Nab2, Mtr4 and the Nab3 subunit of  
198 the NNS complex bind most of mRNAs<sup>4,56</sup>. We retrieved published genomic data for RNA

199 binding (CRAC) for Nab3, Nab2 and Mtr4<sup>4,56</sup>. and corrected their binding to mRNA  
200 transcripts for their respective gene transcription levels as measured by CRAC-Rpb1<sup>56</sup> (Fig.  
201 4a). This normalisation generated an index of Transcript Instability (TI) values for all  
202 protein-coding genes, allowing us to quantitatively assess the level of premature transcription  
203 termination taking place within each mRNA gene.

204 We evaluated whether accumulation of Pol II at the promoter-proximal region is associated  
205 with premature termination. TI values were calculated for the promoter-proximal region (TSS  
206 to TSS+200) and the downstream gene body (TSS+200 to PAS). Genes were clustered in  
207 four groups based on their TR values in WT conditions (Fig. 4b) and  $TIs^{Mtr4/Nab3/Nab2}$  were  
208 analysed for the genes of each group. Intriguingly, a reciprocal relationship between TR and  
209 promoter-proximal TI was observed: genes with increased accumulation of Pol II at the  
210 promoter-proximal region relative to the gene body (low TR) had high  $TIs^{Mtr4/Nab3/Nab2}$ , while  
211 genes with little or no promoter-proximal accumulation of Pol II (high TR) had low TI (Fig.  
212 4c). Contrary, no decrease in the  $TIs^{Mtr4/Nab3/Nab2}$  values was observed within the gene body in  
213 the four TR groups (Fig. 4c). Therefore, defective progression of Pol II from the promoter-  
214 proximal region correlates with early transcription termination at the same region.

### 215 **Functional and physical interactions link INO80 to RNA quality control and NNS-** 216 **dependent transcription termination pathway**

217 Since in *ino80Δ* cells Pol II is stalled at genomic sites associated with increased binding of  
218 RNA surveillance factors to RNA, we interrogated whether the role of INO80 in gene  
219 expression is functionally linked to the RNA quality control process. Abd1 is an essential  
220 m7G cap methyltransferase that prevents mRNA destabilization and degradation<sup>57</sup>. Deletion  
221 of *ARP8* in the *abd1-DAmP* strain, which expresses a hypomorphic allele of *ABD1*<sup>58</sup>, led to  
222 synthetic lethality in non-permissive conditions (Fig. 5a), suggesting that INO80 is essential  
223 for cellular viability when mRNAs are destabilized. Deletion of *ARP8* in the *nrđ1-V368G*

224 (designated as *nrd1-5*) mutant strain, which is deficient in transcription termination<sup>8</sup> led to  
225 synthetic lethality in 6-AU (Fig. 5b). In addition, the *arp8Δ* and *nrd1-5* mutants were  
226 epistatic for *INO1* expression (Fig. 5c) suggesting that the INO80 and NNS complexes work  
227 in the same pathway in gene regulation. These genetic interactions link INO80 to co-  
228 transcriptional RNA quality control, prompting us to test whether the INO80 complex  
229 physically associates with the transcription termination machinery.

230 Protein co-immunoprecipitation analysis after nucleic acid removal demonstrated that the  
231 INO80 complex physically interacts with both Nrd1 and Nab2 *in vivo* (Fig. 5d, e). Contrary,  
232 we could not detect a physical interaction between the INO80 complex and the component of  
233 cleavage and polyadenylation factor IA (CF IA) complex Pcf11 (Extended Data Fig. 4a),  
234 which promotes transcription termination at the PAS.

### 235 **INO80 promotes NNS-dependent transcription termination**

236 To explore the possibility that INO80 is involved in Nrd1-dependent termination, we  
237 employed the well-characterized *ACT-SNR<sup>TTS</sup>-CUP* reporter system<sup>8,59</sup> (Extended Data Fig.  
238 5a). Briefly, cells were transformed with ACT-CUP plasmids without or with the  
239 Transcription Termination Site (TTS) of the snoRNA gene *SNR13* (*SNR<sup>TTS</sup>*) inserted prior to  
240 the CUP1 gene, which confers resistance to copper. Termination of snoRNAs, including  
241 *SNR13*, is regulated by the NNS complex<sup>8,60</sup>. INO80 is co-enriched with Nrd1 at the  
242 endogenous *SNR13<sup>TTS</sup>* region (Extended Data Fig. 4b), making the *ACT-SNR<sup>TTS</sup>-CUP*  
243 reporter a suitable system to test the role of INO80 in NNS-dependent transcription  
244 termination. Contrary to WT, *ino80Δ* cells transformed with the *ACT-SNR<sup>TTS</sup>-CUP* plasmid  
245 were able to grow in the presence of copper, suggesting read-through transcription of *CUP1*  
246 (Fig. 6a). RT-qPCR analysis using primer pairs that target the regions before and after the  
247 *SNR13<sup>TTS</sup>* insertion site in the reporter plasmids showed a significant increase in the relative  
248 transcription of *CUP1* in the *ACT-SNR<sup>TTS</sup>-CUP* plasmid in *ino80Δ* and *arp8Δ* mutants by 2.8-

249 fold and 3.5-fold respectively (Fig. 6b and Extended Data Fig. 5c). Similarly, a 3-fold  
250 increase was observed in *nrd1-5* cells, in accordance to previous studies<sup>8</sup> (Fig. 6b and  
251 Extended Data Fig. 5c). Inducible degradation of Ino80 also resulted in an acute increase in  
252 relative *CUP1* levels from the *ACT-SNR<sup>TTS</sup>-CUP* but not from the control *ACT-CUP* plasmid  
253 lacking the transcription termination site (Extended Data Fig. 5d). Deletion of either *INO80*  
254 or *ARP8* did not significantly alter gene expression of any of the known transcription  
255 termination and RNA surveillance factors (Extended Data Table 2). These results support a  
256 direct role for INO80 in transcription termination at the *SNR13<sup>TTS</sup>* termination site.

257 To further substantiate a role for INO80 in NNS-dependent termination, we evaluated read-  
258 through transcription at the termination sites of endogenous snoRNA genes. Using paired-  
259 end, spiked-in RNA sequencing we mapped the sense RNA-seq reads encompassing the TTS  
260 of the snoRNA genes in WT and *ino80Δ*. In the absence of INO80 read-through transcripts  
261 are significantly increased for the majority of the snoRNA genes, but not for the ribosomal  
262 protein coding gene *YNL096C* (Fig. 6c, d, and Extended Data Fig. 5e and Extended Data  
263 Table 3). The increase in readthrough transcripts in *ino80Δ* is not due to defective  
264 degradation, as termination of snoRNAs in cells deleted for the 5'-3' exoribonuclease *XRNI*  
265 was normal, while deletion of the nuclear exosome subunit *RRP6* compromised termination  
266 only at a small number of specific snoRNA genes, in accordance with previous studies<sup>61,62</sup>  
267 (Fig. 6d and Extended Data Table 2). These results suggest that INO80 promotes NNS-  
268 dependent transcription termination.

269 To investigate the effect of INO80 loss on premature termination of mRNA synthesis, we  
270 focused our analysis on the *NRD1* gene, which is a known target for promoter-proximal  
271 transcription termination by the NNS/Rrp6 pathway<sup>8,61</sup>. Ino80 is enriched at the promoter-  
272 proximal region of *NRD1* (Extended Data Fig. 5f) and loss of INO80 resulted in increased  
273 promoter-proximal Pol II density at *NRD1* compared to WT (Extended Data Fig. 5g). To

274 assess termination proximally to promoters and at the end of the gene we conducted  
275 quantitative 3' rapid amplification of cDNA ends (3' RACE) using gene-specific primers for  
276 either the promoter-proximal or the PAS region of the *NRDI* gene respectively. Deletion of  
277 *RRP6* increased the relative abundance of promoter-proximally terminated *NRDI* mRNAs  
278 compared to WT, while also upregulated the expression of *NRDI* transcripts terminated at the  
279 end of the gene, in line with RNA-seq data (Fig. 6e and Extended Data Fig. 5h). Notably,  
280 deletion of either *INO80* or *APR8* attenuated the expression of early terminated transcripts  
281 compared to the PAS-terminated *NRDI* transcripts (Fig. 6e). This suggests that the INO80  
282 complex promotes premature transcription termination at mRNA genes.

### 283 **INO80 promotes chromatin recruitment and association of Nab2 with H2A.Z**

284 To understand the mechanism underlying the function of INO80 in premature termination,  
285 we hypothesized that INO80 regulates the recruitment of the RNA quality control machinery  
286 to chromatin. The RNA surveillance factor Nab2 promotes transcription termination<sup>50</sup>. Nab2  
287 binds promoter-proximal mRNAs that are prematurely terminated<sup>4</sup>, including *NRDI*  
288 (Extended Data Fig. 6a), while it is co-transcriptionally recruited to the gene body of actively  
289 transcribed mRNA genes<sup>12</sup>. We therefore tested by ChIP-qPCR whether association of Nab2  
290 with chromatin depends on INO80. Co-transcriptional recruitment of Nab2 to the promoter-  
291 proximal region of *NRDI* was reduced in the absence of INO80 (Fig. 7a and Extended Data  
292 Fig. 6b). Likewise, Nab2 co-transcriptional recruitment at the *SNR13* gene was also  
293 compromised in *ino80Δ* (Extended Data Fig. 6c). Co-immunoprecipitation for Nab2  
294 confirmed that the physical interaction between Nab2 and Rpb1 was independent of INO80  
295 (Extended Data Fig. 6d), excluding the possibility that the decreased recruitment of Nab2 to  
296 chromatin is caused by compromised binding to the Pol II machinery. To evaluate whether  
297 loss of INO80 disrupts the association of Nab2 with the promoter-proximal *NRDI* transcript,  
298 we conducted quantitative RNA-IP for Nab2. In *ino80Δ* cells the binding of Nab2 to

299 promoter-proximal *NRDI* RNA was significantly reduced compared to its binding to the  
300 PAS-proximal *NRDI* region (3'-*NRDI*) (Fig. 7b). These results suggest that INO80 regulates  
301 recruitment of Nab2 to chromatin to promote its binding to nascent RNAs.

302 We sought to gain insight into how INO80 promotes recruitment of Nab2 to chromatin.  
303 Promoter-proximal nucleosomes are enriched in the histone variant H2A.Z<sup>63</sup>. H2A.Z has  
304 been suggested to have a role in RNA quality control and non-PAS transcription termination  
305 in *D.melanogaster* and *S.pombe*<sup>64-66</sup>. INO80 preferentially remodels nucleosomes containing  
306 H2A.Z and controls the dynamic association of H2A.Z with chromatin<sup>33,67-69</sup>, raising the  
307 possibility that H2A.Z might be involved in NNS-dependent termination. Cells lacking  
308 *HTZI*, which encodes for H2A.Z in budding yeast, grew in the presence of copper when  
309 transformed with the *ACT-SNR<sup>TTS</sup>-CUP* plasmid (Fig.7c and Extended Data Fig. 6f),  
310 suggesting that H2A.Z suppresses read-through transcription from NNS-dependent  
311 termination sites. Promoter-proximally terminated *NRDI* transcripts were decreased in *htz1Δ*  
312 compared to WT (Fig. 7d), indicating that loss of H2A.Z compromises premature  
313 transcription termination of mRNA genes. In line with defective early termination, co-  
314 transcriptional recruitment of Nab2 at the promoter-proximal region of *NRDI* was reduced in  
315 *htz1Δ* cells (Fig. 7e and Extended Data Fig. 6g). Co-immunoprecipitation assays after nucleic  
316 acid removal demonstrated that H2A.Z interacts with Nab2, even after non-physiological  
317 high-salt wash conditions, but not with Pcf11 (Fig. 7f and Extended Data Fig. 7h, i). Since  
318 our evidence indicate that H2A.Z is involved in premature transcription termination and RNA  
319 quality control at mRNA genes, we asked whether INO80 controls the interaction between  
320 H2A.Z and Nab2. Remarkably, binding of Nab2 to H2A.Z was decreased in *ino80Δ* (Fig. 7f).  
321 This suggests that INO80 enables the recruitment of the Nab2 RNA surveillance machinery  
322 to chromatin by promoting its interaction with H2A.Z.

## 323 **DISCUSSION**

324 Here, we elucidate a role for INO80 in transcription. We report that INO80 enables  
325 recruitment of the RNA quality control machinery to transcribed mRNA genes for early  
326 transcription termination, promoting transcription elongation. Our data suggest that by  
327 removal of Pol II and termination of unproductive transcription, INO80 defines a chromatin-  
328 based pathway for co-transcriptional mRNA quality control. Based on our results we propose  
329 that control of premature transcriptional termination by INO80-dependent chromatin  
330 remodelling is a genome-wide regulatory mechanism of eukaryotic gene expression.

### 331 **Linking mRNA quality control to chromatin regulation**

332 What is the role of Pol II accumulation at the promoter-proximal region? Our analysis links  
333 promoter-proximal accumulation of Pol II with RNA surveillance and transcription  
334 termination. Binding of the RNA quality control factors Nab3, Mtr4 and Nab2 to mRNA  
335 transcripts is enhanced at promoter-proximal regions. Therefore, a model emerges that  
336 increased dwelling of Pol II at specific promoter-proximal sites provides the time for RNA  
337 surveillance and termination factors to be loaded to nascent transcripts efficiently. Our  
338 cumulative findings that in the absence of INO80 (i) Pol II accumulates at promoter proximal  
339 regions, (ii) Nab2 recruitment to chromatin and binding to RNA are defective and (iii) early  
340 termination is compromised, suggest that removal of Pol II molecules that are not engaged in  
341 productive transcription is mediated by INO80. Given that loss of INO80 results in reduced  
342 transcription rates, our results substantiate the hypothesis that chromatin promotes  
343 transcription by orchestrating the co-transcriptional RNA quality control pathway. It is  
344 therefore tempting to speculate that chromatin acts as a molecular switch that dictates  
345 whether Pol II will either progress into productive elongation or be removed to allow for the  
346 next round of transcription to take place.

### 347 **Chromatin regulation of premature transcription termination by INO80**

348 How does INO80 promote premature termination? The physical interactions of the INO80  
349 complex with the transcription termination and RNA surveillance factors Nrd1 and Nab2, and  
350 the enrichment of INO80 at NNS-dependent termination regions suggest a direct involvement  
351 for INO80 in the co-transcriptional RNA quality control pathway. Nab2 associates with the  
352 RNA cleavage factor Hrp1<sup>70</sup> and both factors are involved in mRNA quality control and  
353 NNS-dependent termination<sup>4,71,72</sup>. The INO80-dependent recruitment of Nab2 to chromatin  
354 could therefore promote co-transcriptional cleavage of the nascent RNA, leading to  
355 destabilization of the transcription elongation complex and subsequent release of Pol II from  
356 chromatin. As INO80 interacts with and facilitates release of poly-ubiquitinated Rpb1 from  
357 chromatin<sup>35</sup>, an intriguing possibility is that Rpb1 ubiquitination is involved in the process,  
358 providing specificity for selective eviction of Pol II molecules by INO80.

359 In agreement with a role for H2A.Z in RNA quality control and non-poly(A) transcription  
360 termination<sup>64-66</sup>, our results suggest that INO80 promotes recruitment of Nab2 to chromatin  
361 by regulating its interaction with H2A.Z (Figure 7). This implies that remodelling of H2A.Z-  
362 containing nucleosomes by INO80<sup>67-69</sup> is important for premature termination. It is therefore  
363 likely that intermediate steps in the H2A.Z exchange reaction by INO80, for example  
364 disposing of DNA from the surface of H2A.Z-H2B dimers<sup>69</sup>, might be involved in the  
365 process. How H2A.Z promotes recruitment of the RNA quality control machinery to  
366 chromatin is not clear. It would not be surprising if regulation of premature termination  
367 entails posttranslational modifications on H2A.Z, which would command its role in the RNA  
368 quality control pathway.

369 Promoter-proximal transcriptional pausing has recently been linked to premature termination  
370 in metazoans<sup>6,19-21</sup>. Uncontrolled transcription elongation and dysregulated Pol II pausing  
371 have been implicated in human disease<sup>73,74</sup>. Mutations in the RNA surveillance machinery  
372 have been associated with increased transcriptional stress and genomic instability<sup>75</sup>, both

373 hallmarks of cancer<sup>76</sup>. Dysregulated expression of INO80 leads to uncontrolled gene  
374 expression and is associated with disease<sup>31,77,78</sup>. We therefore anticipated that our reported  
375 chromatin mechanism of co-transcriptional RNA quality control has general relevance for  
376 regulation of eukaryotic gene expression and in disease.

377 **Competing interests**

378 The authors declare that they have no competing interests. BFP has a financial interest in  
379 Peconic, LLC, which utilizes the ChIP-exo technology implemented in this study and could  
380 potentially benefit from the outcomes of this research.

381 **Funding**

382 MPC is supported by Newcastle and Liverpool University. AM is supported by the Agence  
383 Nationale de la Recherche (ANR) (DNA-Life) and the European Research Council  
384 (EPIncrRNA starting grant, DARK consolidator grant). This work has received support from  
385 the U.S. National Institutes of Health HG004160 to BFP, and from the ANR (AAPG2019  
386 PICen to L.T., ANR-18-CE12-0026 and ANR-20-CE12-0014-02 to D.D.).

387 **Acknowledgements**

388 We thank D. Shapira (Newcastle University) for assisting with experiments and constructive  
389 discussions. We thank S. Baulande and P. Legoix-Né (NGS platform, Institute Curie). We  
390 also thank Maxime Wéry and Nicolas Vogt for outstanding help with the NET-seq and RNA-  
391 seq assays and critical reading of the manuscript, David A. Brow for the generous gift of the  
392 pGAC24 and pGAC24-SNR13TTS plasmids and the *nr1-5* yeast strain, and Kuangyu Yen,  
393 Lisa Prendergast and members of the Papamichos-Chronakis and Morillon's labs for  
394 constructive discussions. This work has benefited from the facilities and expertise of the NGS  
395 platform of Institute Curie, supported by the Agence Nationale de la Recherche (ANR-10-  
396 EQPX-03, ANR10-INBS-09-08) and the Canceropôle Ile-de-France.

397 **References**

- 398 1. Porrua, O. & Libri, D. RNA quality control in the nucleus: the Angels' share of RNA.  
399 *Biochim Biophys Acta* **1829**, 604-11 (2013).
- 400 2. Pelechano, V., Chavez, S. & Perez-Ortin, J.E. A complete set of nascent transcription  
401 rates for yeast genes. *PLoS One* **5**, e15442 (2010).
- 402 3. Kim, T.S. et al. RNA polymerase mapping during stress responses reveals widespread  
403 nonproductive transcription in yeast. *Genome Biol* **11**, R75 (2010).
- 404 4. Tuck, A.C. & Tollervey, D. A transcriptome-wide atlas of RNP composition reveals  
405 diverse classes of mRNAs and lncRNAs. *Cell* **154**, 996-1009 (2013).
- 406 5. Bresson, S. & Tollervey, D. Surveillance-ready transcription: nuclear RNA decay as a  
407 default fate. *Open Biol* **8**(2018).
- 408 6. Steurer, B. et al. Live-cell analysis of endogenous GFP-RPB1 uncovers rapid turnover  
409 of initiating and promoter-paused RNA Polymerase II. *Proc Natl Acad Sci U S A* **115**,  
410 E4368-E4376 (2018).
- 411 7. Darzacq, X. et al. In vivo dynamics of RNA polymerase II transcription. *Nat Struct Mol*  
412 *Biol* **14**, 796-806 (2007).
- 413 8. Steinmetz, E.J., Conrad, N.K., Brow, D.A. & Corden, J.L. RNA-binding protein Nrd1  
414 directs poly(A)-independent 3'-end formation of RNA polymerase II transcripts.  
415 *Nature* **413**, 327-31 (2001).
- 416 9. Kilchert, C., Wittmann, S. & Vasiljeva, L. The regulation and functions of the nuclear  
417 RNA exosome complex. *Nat Rev Mol Cell Biol* **17**, 227-39 (2016).
- 418 10. Jensen, T.H., Jacquier, A. & Libri, D. Dealing with pervasive transcription. *Mol Cell* **52**,  
419 473-84 (2013).
- 420 11. Mayer, A. et al. CTD tyrosine phosphorylation impairs termination factor recruitment  
421 to RNA polymerase II. *Science* **336**, 1723-5 (2012).
- 422 12. Gonzalez-Aguilera, C. et al. Nab2 functions in the metabolism of RNA driven by  
423 polymerases II and III. *Mol Biol Cell* **22**, 2729-40 (2011).
- 424 13. Yu, M.C. et al. Arginine methyltransferase affects interactions and recruitment of  
425 mRNA processing and export factors. *Genes Dev* **18**, 2024-35 (2004).
- 426 14. Bresson, S., Tuck, A., Staneva, D. & Tollervey, D. Nuclear RNA Decay Pathways Aid  
427 Rapid Remodeling of Gene Expression in Yeast. *Mol Cell* **65**, 787-800 e5 (2017).
- 428 15. Webb, S., Hector, R.D., Kudla, G. & Granneman, S. PAR-CLIP data indicate that Nrd1-  
429 Nab3-dependent transcription termination regulates expression of hundreds of  
430 protein coding genes in yeast. *Genome Biol* **15**, R8 (2014).
- 431 16. Schulz, D. et al. Transcriptome surveillance by selective termination of noncoding  
432 RNA synthesis. *Cell* **155**, 1075-87 (2013).
- 433 17. Kapranov, P. et al. RNA maps reveal new RNA classes and a possible function for  
434 pervasive transcription. *Science* **316**, 1484-8 (2007).
- 435 18. Yu, D., Ma, X., Zuo, Z., Wang, H. & Meng, Y. Classification of Transcription Boundary-  
436 Associated RNAs (TBARs) in Animals and Plants. *Front Genet* **9**, 168 (2018).
- 437 19. Chiu, A.C. et al. Transcriptional Pause Sites Delineate Stable Nucleosome-Associated  
438 Premature Polyadenylation Suppressed by U1 snRNP. *Mol Cell* **69**, 648-663 e7  
439 (2018).
- 440 20. Erickson, B., Sheridan, R.M., Cortazar, M. & Bentley, D.L. Dynamic turnover of  
441 paused Pol II complexes at human promoters. *Genes Dev* (2018).

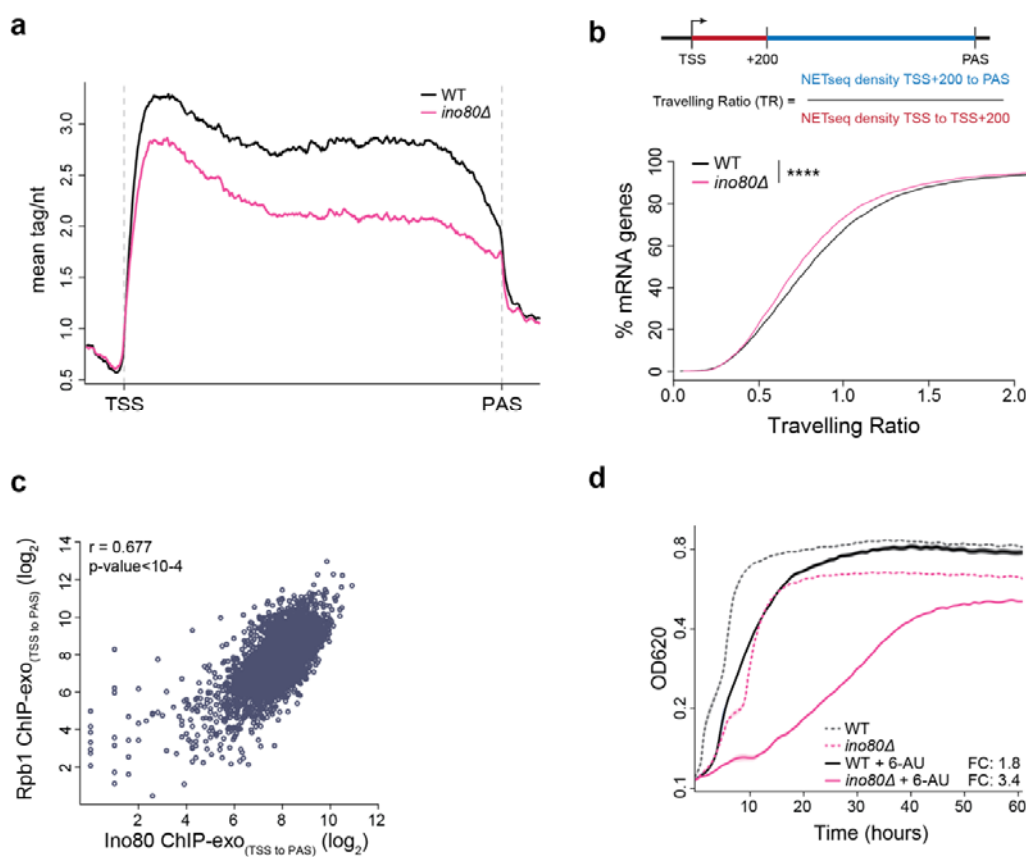
- 442 21. Krebs, A.R. et al. Genome-wide Single-Molecule Footprinting Reveals High RNA  
443 Polymerase II Turnover at Paused Promoters. *Mol Cell* **67**, 411-422 e4 (2017).
- 444 22. Gressel, S. et al. CDK9-dependent RNA polymerase II pausing controls transcription  
445 initiation. *Elife* **6**(2017).
- 446 23. Shao, W. & Zeitlinger, J. Paused RNA polymerase II inhibits new transcriptional  
447 initiation. *Nat Genet* **49**, 1045-1051 (2017).
- 448 24. Chen, F.X., Smith, E.R. & Shilatifard, A. Born to run: control of transcription  
449 elongation by RNA polymerase II. *Nat Rev Mol Cell Biol* (2018).
- 450 25. Taft, R.J., Kaplan, C.D., Simons, C. & Mattick, J.S. Evolution, biogenesis and function  
451 of promoter-associated RNAs. *Cell Cycle* **8**, 2332-8 (2009).
- 452 26. Whitehouse, I., Rando, O.J., Delrow, J. & Tsukiyama, T. Chromatin remodelling at  
453 promoters suppresses antisense transcription. *Nature* **450**, 1031-5 (2007).
- 454 27. Boeger, H., Griesenbeck, J. & Kornberg, R.D. Nucleosome retention and the  
455 stochastic nature of promoter chromatin remodeling for transcription. *Cell* **133**, 716-  
456 26 (2008).
- 457 28. Smolle, M. et al. Chromatin remodelers Isw1 and Chd1 maintain chromatin structure  
458 during transcription by preventing histone exchange. *Nat Struct Mol Biol* **19**, 884-92  
459 (2012).
- 460 29. Morillon, A. et al. Isw1 chromatin remodeling ATPase coordinates transcription  
461 elongation and termination by RNA polymerase II. *Cell* **115**, 425-35 (2003).
- 462 30. Babour, A. et al. The Chromatin Remodeler ISW1 Is a Quality Control Factor that  
463 Surveys Nuclear mRNP Biogenesis. *Cell* **167**, 1201-1214 e15 (2016).
- 464 31. Poli, J., Gasser, S.M. & Papamichos-Chronakis, M. The INO80 remodeler in  
465 transcription, replication and repair. *Philos Trans R Soc Lond B Biol Sci* **372**(2017).
- 466 32. Xue, Y. et al. Mot1, Ino80C, and NC2 Function Coordinately to Regulate Pervasive  
467 Transcription in Yeast and Mammals. *Mol Cell* **67**, 594-607 e4 (2017).
- 468 33. Yen, K., Vinayachandran, V. & Pugh, B.F. SWR-C and INO80 chromatin remodelers  
469 recognize nucleosome-free regions near +1 nucleosomes. *Cell* **154**, 1246-56 (2013).
- 470 34. Poli, J. et al. Mec1, INO80, and the PAF1 complex cooperate to limit transcription  
471 replication conflicts through RNAPII removal during replication stress. *Genes Dev* **30**,  
472 337-54 (2016).
- 473 35. Lafon, A. et al. INO80 Chromatin Remodeler Facilitates Release of RNA Polymerase II  
474 from Chromatin for Ubiquitin-Mediated Proteasomal Degradation. *Mol Cell* **60**, 784-  
475 96 (2015).
- 476 36. Tsvetanova, N.G., Klass, D.M., Salzman, J. & Brown, P.O. Proteome-wide search  
477 reveals unexpected RNA-binding proteins in *Saccharomyces cerevisiae*. *PLoS One*  
478 **5**(2010).
- 479 37. Edupuganti, R.R. et al. N(6)-methyladenosine (m(6)A) recruits and repels proteins to  
480 regulate mRNA homeostasis. *Nat Struct Mol Biol* **24**, 870-878 (2017).
- 481 38. Churchman, L.S. & Weissman, J.S. Nascent transcript sequencing visualizes  
482 transcription at nucleotide resolution. *Nature* **469**, 368-73 (2011).
- 483 39. Wissink, E.M., Vihervaara, A., Tippens, N.D. & Lis, J.T. Nascent RNA analyses: tracking  
484 transcription and its regulation. *Nat Rev Genet* (2019).
- 485 40. Harlen, K.M. & Churchman, L.S. Subgenic Pol II interactomes identify region-specific  
486 transcription elongation regulators. *Mol Syst Biol* **13**, 900 (2017).

- 487 41. Yen, K., Vinayachandran, V., Batta, K., Koerber, R.T. & Pugh, B.F. Genome-wide  
488 nucleosome specificity and directionality of chromatin remodelers. *Cell* **149**, 1461-73  
489 (2012).
- 490 42. Rhee, H.S. & Pugh, B.F. ChIP-exo method for identifying genomic location of DNA-  
491 binding proteins with near-single-nucleotide accuracy. *Curr Protoc Mol Biol* **Chapter**  
492 **21**, Unit 21 24 (2012).
- 493 43. Shaw, R.J. & Reines, D. *Saccharomyces cerevisiae* transcription elongation mutants  
494 are defective in PUR5 induction in response to nucleotide depletion. *Mol Cell Biol* **20**,  
495 7427-37 (2000).
- 496 44. Ehrensberger, A.H., Kelly, G.P. & Svejstrup, J.Q. Mechanistic interpretation of  
497 promoter-proximal peaks and RNAPII density maps. *Cell* **154**, 713-5 (2013).
- 498 45. Baptista, T. et al. SAGA Is a General Cofactor for RNA Polymerase II Transcription.  
499 *Mol Cell* **68**, 130-143 e5 (2017).
- 500 46. Timmers, H.T.M. & Tora, L. Transcript Buffering: A Balancing Act between mRNA  
501 Synthesis and mRNA Degradation. *Mol Cell* **72**, 10-17 (2018).
- 502 47. Sun, M. et al. Comparative dynamic transcriptome analysis (cDTA) reveals mutual  
503 feedback between mRNA synthesis and degradation. *Genome Res* **22**, 1350-9 (2012).
- 504 48. Malagon, F. et al. Mutations in the *Saccharomyces cerevisiae* RPB1 gene conferring  
505 hypersensitivity to 6-azauracil. *Genetics* **172**, 2201-9 (2006).
- 506 49. Pelechano, V. & Perez-Ortin, J.E. The transcriptional inhibitor thiolutin blocks mRNA  
507 degradation in yeast. *Yeast* **25**, 85-92 (2008).
- 508 50. Alpert, T., Straube, K., Carrillo Oesterreich, F., Herzel, L. & Neugebauer, K.M.  
509 Widespread Transcriptional Readthrough Caused by Nab2 Depletion Leads to  
510 Chimeric Transcripts with Retained Introns. *Cell Rep* **33**, 108324 (2020).
- 511 51. Aguilar, L.C. et al. Altered rRNA processing disrupts nuclear RNA homeostasis via  
512 competition for the poly(A)-binding protein Nab2. *Nucleic Acids Res* **48**, 11675-11694  
513 (2020).
- 514 52. Fasken, M.B., Laribee, R.N. & Corbett, A.H. Nab3 facilitates the function of the  
515 TRAMP complex in RNA processing via recruitment of Rrp6 independent of Nrd1.  
516 *PLoS Genet* **11**, e1005044 (2015).
- 517 53. Fox, M.J. & Mosley, A.L. Rrp6: Integrated roles in nuclear RNA metabolism and  
518 transcription termination. *Wiley Interdiscip Rev RNA* **7**, 91-104 (2016).
- 519 54. Vasiljeva, L. & Buratowski, S. Nrd1 interacts with the nuclear exosome for 3'  
520 processing of RNA polymerase II transcripts. *Mol Cell* **21**, 239-48 (2006).
- 521 55. Tudek, A. et al. Molecular basis for coordinating transcription termination with  
522 noncoding RNA degradation. *Mol Cell* **55**, 467-81 (2014).
- 523 56. Holmes, R.K. et al. Loss of the Yeast SR Protein Npl3 Alters Gene Expression Due to  
524 Transcription Readthrough. *PLoS Genet* **11**, e1005735 (2015).
- 525 57. Schwer, B., Mao, X. & Shuman, S. Accelerated mRNA decay in conditional mutants of  
526 yeast mRNA capping enzyme. *Nucleic Acids Res* **26**, 2050-7 (1998).
- 527 58. Breslow, D.K. et al. A comprehensive strategy enabling high-resolution functional  
528 analysis of the yeast genome. *Nat Methods* **5**, 711-8 (2008).
- 529 59. Arigo, J.T., Carroll, K.L., Ames, J.M. & Corden, J.L. Regulation of yeast NRD1  
530 expression by premature transcription termination. *Mol Cell* **21**, 641-51 (2006).
- 531 60. Kim, M. et al. Distinct pathways for snoRNA and mRNA termination. *Mol Cell* **24**, 723-  
532 734 (2006).

- 533 61. Fox, M.J., Gao, H., Smith-Kinnaman, W.R., Liu, Y. & Mosley, A.L. The exosome  
534 component Rrp6 is required for RNA polymerase II termination at specific targets of  
535 the Nrd1-Nab3 pathway. *PLoS Genet* **11**, e1004999 (2015).
- 536 62. van Dijk, E.L. et al. XUTs are a class of Xrn1-sensitive antisense regulatory non-coding  
537 RNA in yeast. *Nature* **475**, 114-7 (2011).
- 538 63. Albert, I. et al. Translational and rotational settings of H2A.Z nucleosomes across the  
539 *Saccharomyces cerevisiae* genome. *Nature* **446**, 572-6 (2007).
- 540 64. Zofall, M. et al. Histone H2A.Z cooperates with RNAi and heterochromatin factors to  
541 suppress antisense RNAs. *Nature* **461**, 419-22 (2009).
- 542 65. Wagner, E.J. et al. A genome-wide RNA interference screen reveals that variant  
543 histones are necessary for replication-dependent histone pre-mRNA processing. *Mol*  
544 *Cell* **28**, 692-9 (2007).
- 545 66. Muniz, L. et al. Control of Gene Expression in Senescence through Transcriptional  
546 Read-Through of Convergent Protein-Coding Genes. *Cell Rep* **21**, 2433-2446 (2017).
- 547 67. Papamichos-Chronakis, M., Watanabe, S., Rando, O.J. & Peterson, C.L. Global  
548 regulation of H2A.Z localization by the INO80 chromatin-remodeling enzyme is  
549 essential for genome integrity. *Cell* **144**, 200-13 (2011).
- 550 68. Eustermann, S. et al. Structural basis for ATP-dependent chromatin remodelling by  
551 the INO80 complex. *Nature* **556**, 386-390 (2018).
- 552 69. Brahma, S. et al. INO80 exchanges H2A.Z for H2A by translocating on DNA proximal  
553 to histone dimers. *Nat Commun* **8**, 15616 (2017).
- 554 70. Dheur, S., Nykamp, K.R., Viphakone, N., Swanson, M.S. & Minvielle-Sebastia, L. Yeast  
555 mRNA Poly(A) tail length control can be reconstituted in vitro in the absence of  
556 Pab1p-dependent Poly(A) nuclease activity. *J Biol Chem* **280**, 24532-8 (2005).
- 557 71. Kuehner, J.N. & Brow, D.A. Regulation of a eukaryotic gene by GTP-dependent start  
558 site selection and transcription attenuation. *Mol Cell* **31**, 201-11 (2008).
- 559 72. Roth, K.M., Wolf, M.K., Rossi, M. & Butler, J.S. The nuclear exosome contributes to  
560 autogenous control of NAB2 mRNA levels. *Mol Cell Biol* **25**, 1577-85 (2005).
- 561 73. Rahl, P.B. et al. c-Myc regulates transcriptional pause release. *Cell* **141**, 432-45  
562 (2010).
- 563 74. Zhang, X. et al. Attenuation of RNA polymerase II pausing mitigates BRCA1-  
564 associated R-loop accumulation and tumorigenesis. *Nat Commun* **8**, 15908 (2017).
- 565 75. Aguilera, A. & Gomez-Gonzalez, B. Genome instability: a mechanistic view of its  
566 causes and consequences. *Nat Rev Genet* **9**, 204-17 (2008).
- 567 76. Kotsantis, P., Petermann, E. & Boulton, S.J. Mechanisms of Oncogene-Induced  
568 Replication Stress: Jigsaw Falling into Place. *Cancer Discov* **8**, 537-555 (2018).
- 569 77. Zhou, B. et al. INO80 governs superenhancer-mediated oncogenic transcription and  
570 tumor growth in melanoma. *Genes Dev* **30**, 1440-53 (2016).
- 571 78. Zhang, S. et al. INO80 is required for oncogenic transcription and tumor growth in  
572 non-small cell lung cancer. *Oncogene* **36**, 1430-1439 (2017).
- 573 79. Hemming, S.A. et al. RNA polymerase II subunit Rpb9 regulates transcription  
574 elongation in vivo. *J Biol Chem* **275**, 35506-11 (2000).
- 575 80. Riles, L., Shaw, R.J., Johnston, M. & Reines, D. Large-scale screening of yeast mutants  
576 for sensitivity to the IMP dehydrogenase inhibitor 6-azauracil. *Yeast* **21**, 241-8  
577 (2004).

- 578 81. Creamer, T.J. et al. Transcriptome-wide binding sites for components of the  
579 Saccharomyces cerevisiae non-poly(A) termination pathway: Nrd1, Nab3, and Sen1.  
580 *PLoS Genet* **7**, e1002329 (2011).
- 581 82. Jonsson, Z.O., Jha, S., Wohlschlegel, J.A. & Dutta, A. Rvb1p/Rvb2p recruit Arp5p and  
582 assemble a functional Ino80 chromatin remodeling complex. *Mol Cell* **16**, 465-77  
583 (2004).
- 584 83. Wery, M. et al. Nonsense-Mediated Decay Restricts LncRNA Levels in Yeast Unless  
585 Blocked by Double-Stranded RNA Structure. *Mol Cell* **61**, 379-392 (2016).
- 586 84. Wery, M. et al. Native elongating transcript sequencing reveals global anti-  
587 correlation between sense and antisense nascent transcription in fission yeast. *RNA*  
588 **24**, 196-208 (2018).
- 589 85. Baptista, T. & Devys, D. Saccharomyces cerevisiae Metabolic Labeling with 4-  
590 thiouracil and the Quantification of Newly Synthesized mRNA As a Proxy for RNA  
591 Polymerase II Activity. *J Vis Exp* (2018).
- 592 86. Papamichos-Chronakis, M. & Peterson, C.L. The Ino80 chromatin-remodeling enzyme  
593 regulates replisome function and stability. *Nat Struct Mol Biol* **15**, 338-45 (2008).
- 594 87. Rhee, H.S., Bataille, A.R., Zhang, L. & Pugh, B.F. Subnucleosomal structures and  
595 nucleosome asymmetry across a genome. *Cell* **159**, 1377-88 (2014).
- 596

Figure 1



597

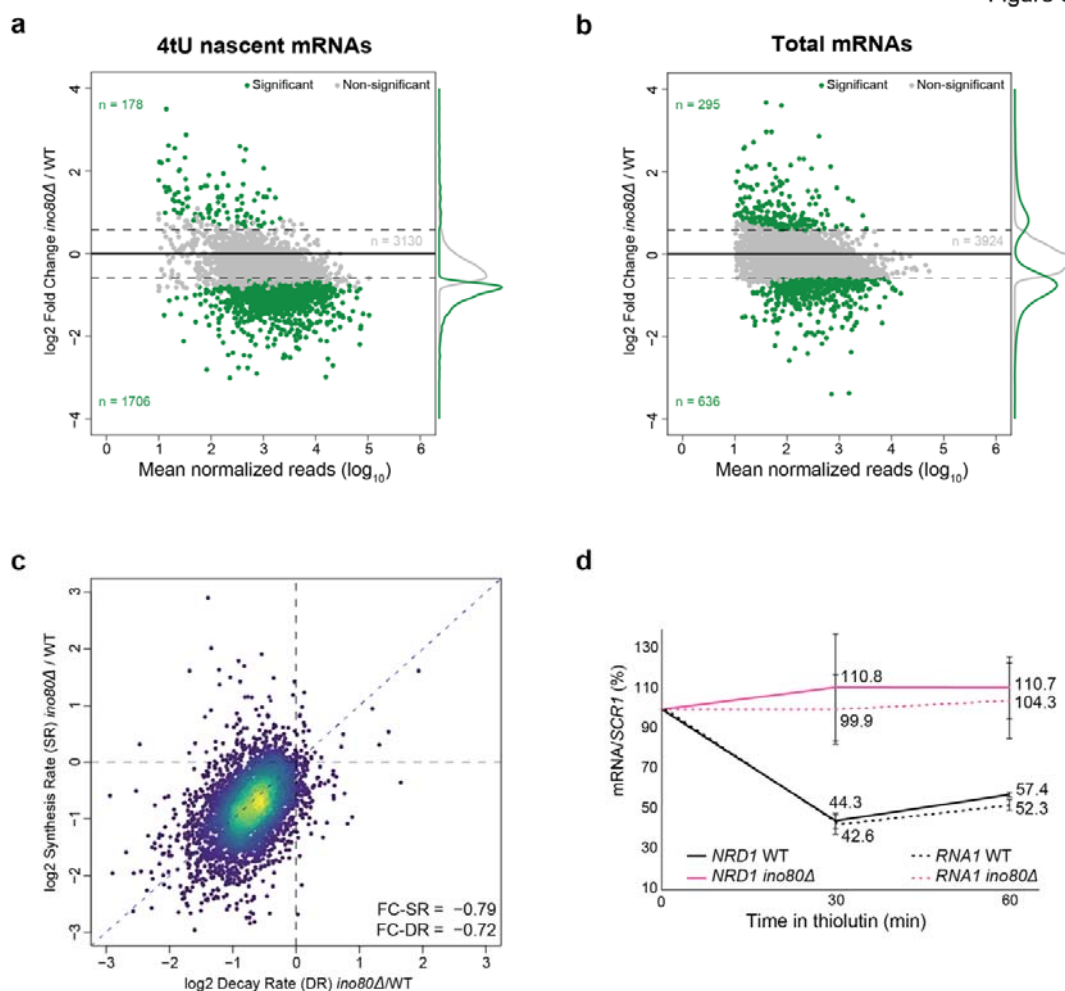
598

599 **Fig. 1. Accumulation of nascent mRNA transcripts on chromatin proximally to**  
 600 **promoters and defective transcriptional elongation in the absence of INO80.**

601 **a**, Metagene analysis for NET-seq density profiles averaged across scaled mRNA genes (n=  
 602 5432) in WT and *ino80Δ*. Tags were aligned to both Transcription Start Site (TSS) and  
 603 Polyadenylation Site (PAS) for each gene. n=2. **b**, Top: Schematic representation and  
 604 formula for calculating the Traveling Ratio (TR) from NET-seq mRNA densities. Bottom:  
 605 Cumulative distribution plot of Traveling Ratio for mRNA genes from a (n=5432). Genes  
 606 with TR>2 (WT: n=354, *ino80Δ*: n=314) are not shown. \*\*\*\*p < 0.0XXX with K-S test. **c**,  
 607 Scatterplot analysis comparing Ino80<sup>33</sup> and Rpb1 ChIP-exo densities between the  
 608 transcription start site and polyadenylation site (TSS to PAS) in mRNA yeast genes  
 609 (n=5798). Pearson's correlation coefficient (r) and p-value are indicated. **d**, Cell proliferation

610 analysis for WT and *ino80Δ* strains grown exponentially in SC-ura and in SC-ura containing  
611 50 μg/ml 6-azauracil (6-AU) liquid media for the indicated time. Cell density was measured  
612 at OD<sup>620</sup> and plotted on a log<sub>2</sub> scale. Doubling time was calculated from OD<sup>620</sup>: 0.2 to OD<sup>620</sup>:  
613 0.4 for all strains in both conditions. Fold Change ratio (FC) of doubling time in 6-AU over  
614 SC-ura for each strain is shown. n=4.

Figure 3



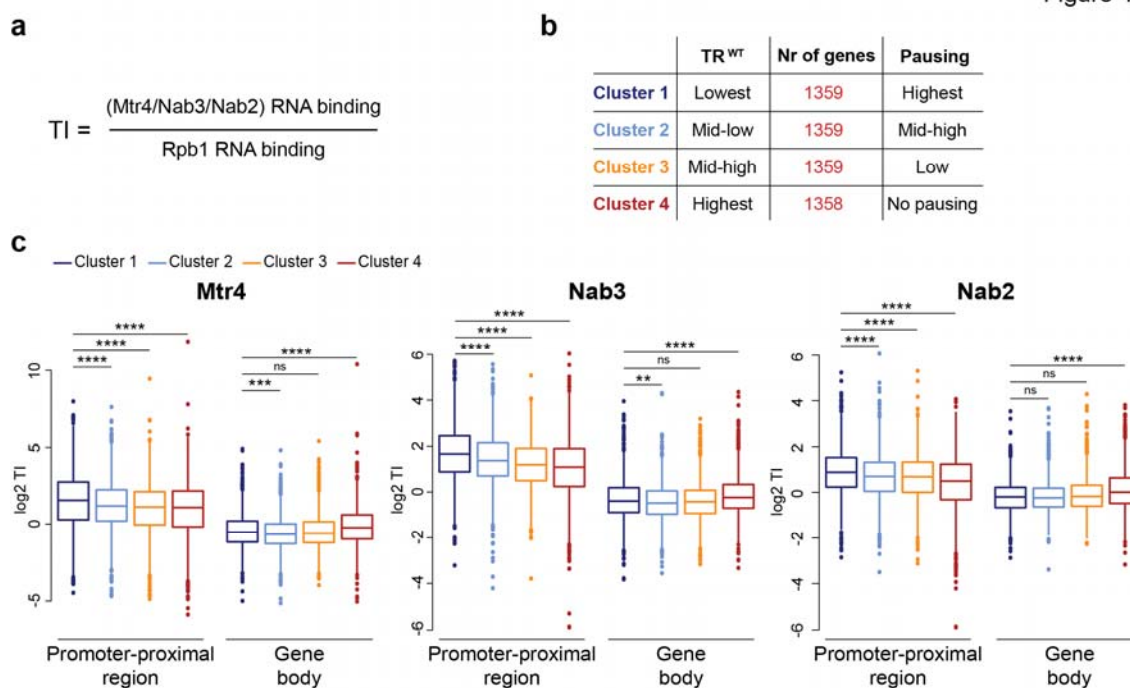
615

616 **Fig. 3. mRNA synthesis and decay rates are reduced in the absence of INO80.**

617 **a, b**, Scatterplot analysis for fold changes between WT and *ino80Δ* in newly synthesized  
 618 mRNA (a) and steady-state mRNA (b) levels (n=5012 genes) plotted on a log<sub>2</sub> scale.  
 619 Thresholds of 1.5-fold change and 0.05 p values were considered for significant change  
 620 (green dots). n=3. **c**, cDTA profiles for *ino80Δ*. For all analysed genes, changes in synthesis  
 621 rates (SR) were plotted against the changes in mRNA decay rates (DR). Fold-change in SR  
 622 and DR were calculated between *ino80Δ* and WT and plotted on a log<sub>2</sub> scale. 90% of genes  
 623 are contained within the outer contour. Yellow and red dots correspond to 60% of genes. **d**,  
 624 RT-qPCR analysis for *NRD1* and *RNA1* RNAs was conducted in WT and *ino80Δ* before (T<sub>0</sub>)  
 625 and after addition of thiolutin in YPD. RNA abundance at each time-point was normalized

626 over the respective abundance of the *SCR1* RNA. RNA before thiolutin treatment was set at  
 627 100% in both strains. Remaining RNA was calculated as the amount of normalized RNA in  
 628 the indicated time-points relative to the normalized RNA at  $T_0$ . Values represent the average  
 629 from at least three independent experiments. Bars, standard errors.

Figure 4



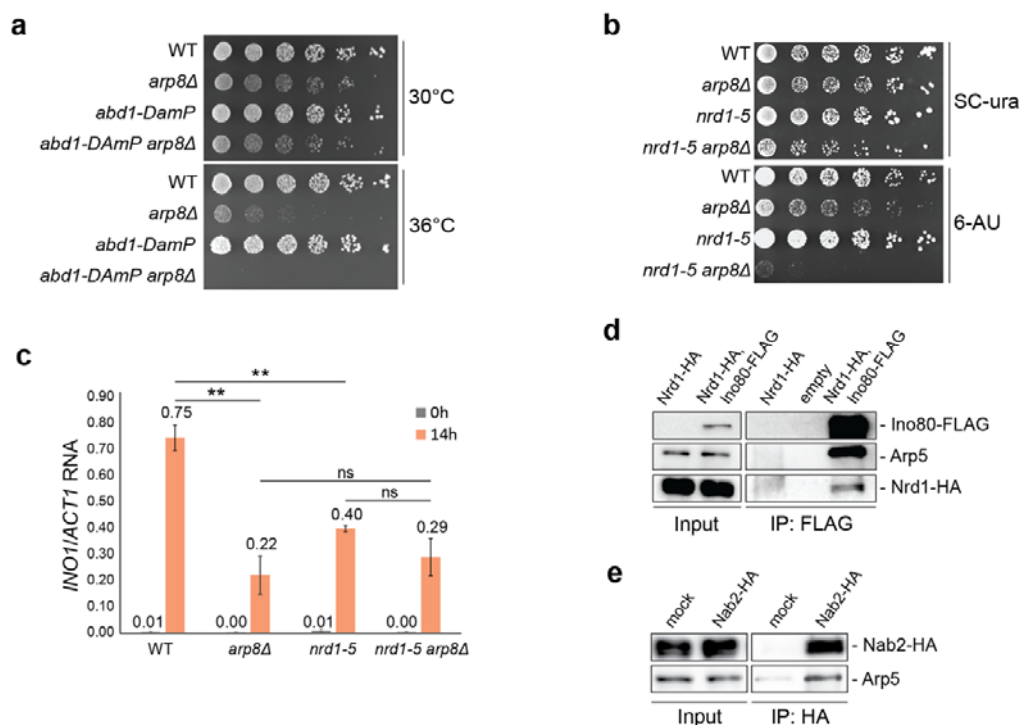
630

631

632 **Fig. 4. Loading of the RNA surveillance and termination factors Mtr4, Nab3 and Nab2**  
 633 **on promoter-proximal mRNA transcripts.**

634 **a**, Formula for calculating Transcript Instability (TI) as the ratio of the averaged CRAC  
 635 densities of Nab3<sup>56</sup>, Mtr4 or Nab2<sup>4</sup> to CRAC densities of Rpb1<sup>56</sup> for mRNA genes. **b**,  
 636 Schematic table for clustering mRNA genes according to the relative TR in WT (TR<sup>WT</sup>). The  
 637 number of genes and the level of promoter-proximal pausing are indicated for each cluster. **c**,  
 638 Boxplot analysis comparing TIs calculated for the promoter-proximal and gene body regions  
 639 of mRNA genes in the four clusters defined by their relative TR<sup>WT</sup>. p-values were calculated  
 640 by Wilcoxon rank-sum test. \*\*\*\*, p<0.0001. \*\*\*, p<0.001. \*\*, p<0.01. ns, non-significant.

Figure 5



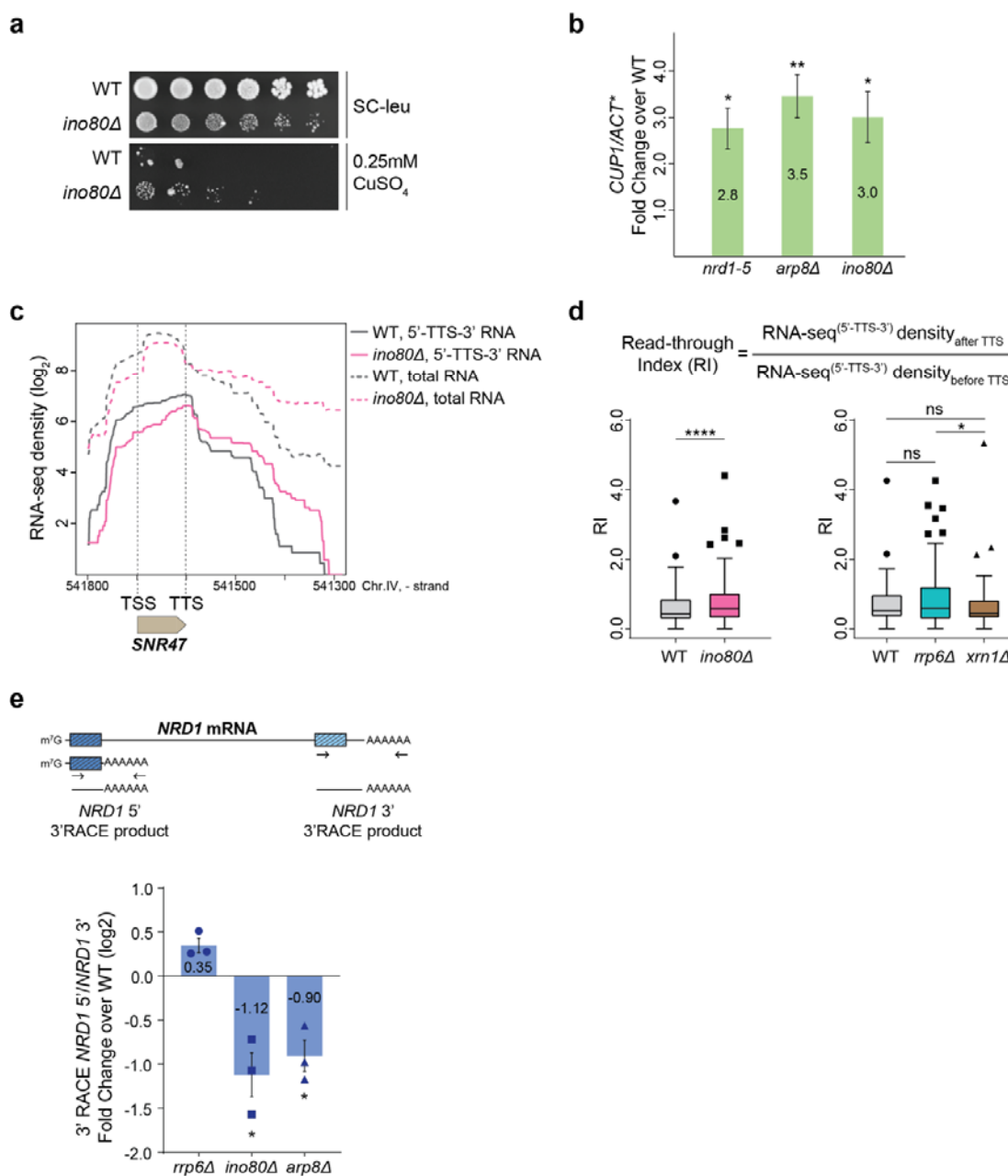
641

642 **Fig. 5. Genetic and physical interactions of INO80 with the RNA quality control**  
 643 **pathway.**

644 **a**, 5-fold serial dilution of exponentially grown cells from the indicated strains were plated  
 645 onto YPD and incubated at 30°C (permissive temperature) or 37°C (non-permissive  
 646 temperature) for 4-5 days. **b**, 5-fold serial dilution of exponentially grown cells from the  
 647 indicated strains were plated onto both SC-ura and SC-ura + 50μg/ml 6-Azaauracil (6-AU)  
 648 and incubated at 30°C for 4-5 days. **c**, RT-qPCR analysis for *INO1* RNA was conducted in  
 649 the indicated strains grown exponentially in SC media (0h) or SC without inositol for 14h.  
 650 *INO1* RNA was normalized over *ACT1* RNA. Bars, standard errors (n=3). Asterisks indicate  
 651 statistical significance of the indicated change as calculated by Tukey's multiple comparisons  
 652 test. ns: non-significant. **d**, Nucleic acid-free lysates from cells co-expressing Nrd1-HA with  
 653 Ino80 either untagged or tagged with FLAG epitope were subjected to FLAG-IP. Inputs and  
 654 IP samples were immunoblotted for FLAG, Arp5, HA. Immunoblot against Pgk1 served as a  
 655 control. **E**, Nucleic acid-free lysates from cells expressing Nab2-HA were subjected to either

656 HA-IP (Nab2-HA) or IgG-IP (mock). Inputs and IP samples were immunoblotted for Arp5  
657 and HA.

Figure 6



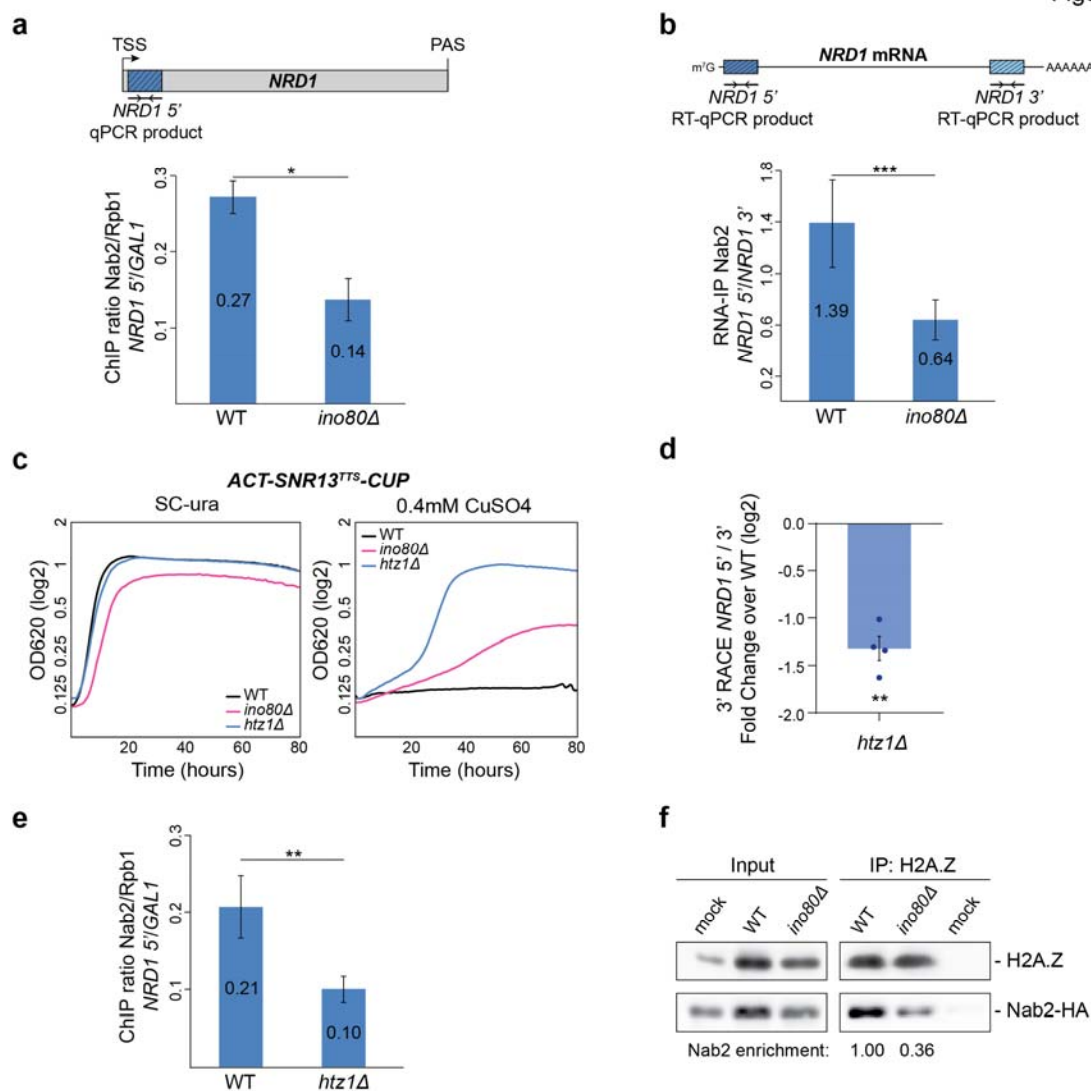
658

659 **Fig. 6. NNS-dependent transcriptional termination is defective in *ino80Δ*.**

660 **a**, 5-fold serial dilution of cells from the indicated strains were plated onto both SC-leu and  
 661 SC-leu + 0.25mM CuSO<sub>4</sub> and incubated at 30°C for 3 (SC-leu) and 7 days (CuSO<sub>4</sub>). **b**, RT-  
 662 qPCR analysis was conducted in WT, *nrd1-5*, *arp8Δ* and *ino80Δ* cells transformed with  
 663 either *ACT-CUP* or *ACT-SNR<sup>TTS</sup>-CUP* plasmids. The *CUP1/ACT\** ratio from the *ACT-*  
 664 *SNR<sup>TTS</sup>-CUP* plasmid was normalized over the same ratio from the control *ACT-CUP*

665 plasmid (Extended Fig. 4c) to correct for differential transcription across all strains. Read-  
666 through at the *SNR13*<sup>TTS</sup> for each indicated strain is shown as Fold Change Ratio over WT.  
667 Bars, standard errors from three independent experiments. p-values were calculated by t-test  
668 after testing for normal distribution by Shapiro-Wilk test. \*, p<0.05. \*\*, p<0.01. **c**, Snapshot  
669 of RNA-seq densities in WT and *ino80Δ* across the *SNR47* snoRNA gene. Solid lines, density  
670 of reads encompassing the transcription termination site (5'-TTS-3') of the *SNR47* gene.  
671 Broken lines, total RNA-seq density. Reads encompassing the TTS were selected from the  
672 total RNA-seq reads as containing 5' upstream the *SNR47* TTS and 3' at or after the *SNR47*  
673 TTS. Genomic coordinates of Chromosome IV around the *SNR47* gene (coordinates: 541700  
674 to 541602) are shown. The closest downstream gene is *YDR042C* (TSS: Chromosome IV,  
675 541203). n=4. **d**, Upper panel, formula for calculating the Read-through Index (RI) from  
676 RNA-seq densities across snoRNA genes that encompass transcription termination sites (5'-  
677 TTS-3'). RNA-seq reads with 5' upstream the TTS and 3' at or after the TTS were selected  
678 from the total RNA-seq read pool and the ratio of the RNA-seq read density after TTS to the  
679 RNA-seq read density before TTS in the selected reads was calculated. Lower panel, boxplot  
680 analysis comparing RI from the indicated strains across snoRNA genes. p-values were  
681 calculated by Wilcoxon matched-pairs rank test after testing for normal distribution. \*\*\*\*\*,  
682 p<0.0001. \*, p<0.05. ns, non-significant. **e**, Top: Scheme illustrating nested 3'RACE for  
683 termination events at the promoter-proximal (5') and PAS (3') regions of the *NRD1* gene  
684 (*NRD1* 5', dark blue). Bottom: 3'RACE analysis for *NRD1* termination events was conducted  
685 in WT and the indicated mutant strains. The relative enrichment of polyadenylated promoter-  
686 proximal to PAS-terminated transcripts (5'/3') was calculated for all strains and the fold  
687 change in each mutant compared to WT was plotted on a log<sub>2</sub> scale. n=3. p-values were  
688 calculated by t-test after testing for normal distribution by Shapiro-Wilk test. \*, p<0.05.

Figure 7



689

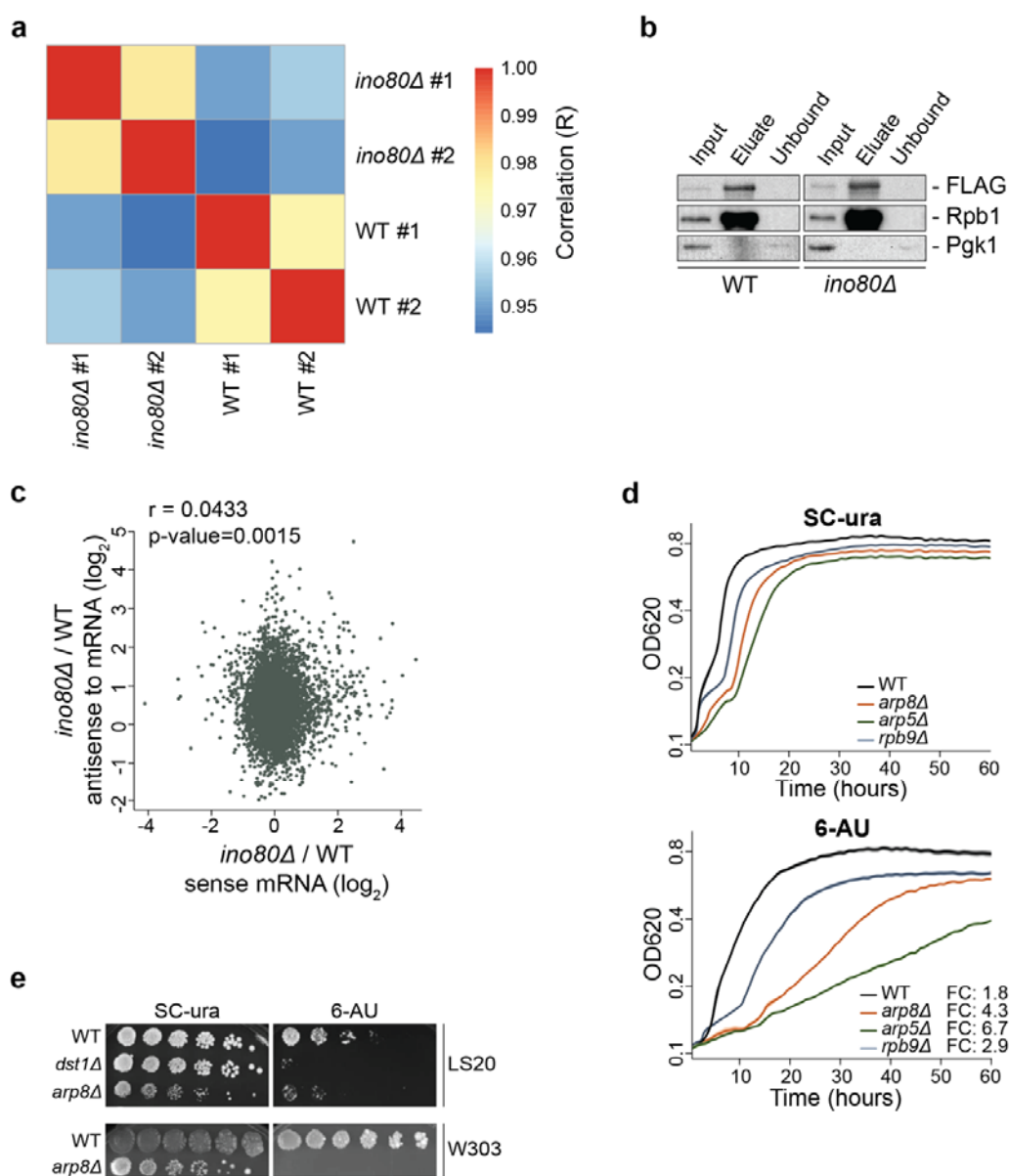
690

691 **Fig. 7. INO80 promotes the co-transcriptional recruitment of Nab2 to chromatin and its**  
 692 **association with H2A.Z.**

693 **a**, Chromatin immunoprecipitation for Nab2-HA and Rpb1 in WT and *ino80Δ* cells. Fold  
 694 enrichment of each protein at the promoter-proximal region of *NRD1* gene (*NRD1* 5') (upper  
 695 panel, shaded in dark blue) was calculated relative to the *GAL1* promoter after correction for  
 696 input DNA levels. ChIP ratio at the promoter-proximal region of *NRD1* gene (*NRD1* 5') was  
 697 calculated as Fold enrichment of Nab2-HA over Fold enrichment of Rpb1. Bars, standard

698 errors from four independent experiments. p-values were calculated by t-test after testing for  
699 normal distribution by Shapiro-Wilk test. \*,  $p < 0.05$ . **b**, RNA immunoprecipitation for Nab2-  
700 HA in WT and *ino80Δ* cells. Ratio of binding of Nab2 to the promoter-proximal *NRDI* RNA  
701 (upper panel, *NRDI* 5', dark blue) over binding to the 3' region of *NRDI* RNA (upper panel,  
702 *NRDI* 3', light blue) after correction for input (total) RNA levels in the indicated strains.  
703 Bars, standard errors from four independent experiments. p-values were calculated by t-test  
704 after testing for normal distribution by Shapiro-Wilk test. \*\*\*,  $p < 0.001$ . **c**, Cell proliferation  
705 analysis for the indicated strains transformed with the *ACT-SNR<sup>TTS</sup>-CUP* plasmid grown  
706 exponentially in SC-ura (left panel) and in SC-ura liquid media containing 0.4mM CuSO<sub>4</sub> (6-  
707 AU) (right panel) for the indicated time. Cell density was measured at OD<sup>620</sup> and is shown on  
708 a log<sub>2</sub> scale. **d**, Nested 3'RACE analysis for termination events at the *NRDI* gene was  
709 conducted in WT and *htz1Δ*. Analysis was conducted as in Fig. 6e. n=4. p-values were  
710 calculated by t-test after testing for normal distribution by Shapiro-Wilk test. \*\*,  $p < 0.01$ . **e**,  
711 Chromatin immunoprecipitation for Nab2-HA and Rpb1 in WT and *htz1Δ* cells. Analysis was  
712 conducted as in (a). Bars, standard errors from three independent experiments. p-values were  
713 calculated by t-test after testing for normal distribution by Shapiro-Wilk test. \*\*,  $p < 0.01$ . **f**,  
714 Representative H2A.Z immunoprecipitation experiment. Nucleic acid-free lysates from WT  
715 and *ino80Δ* cells expressing Nab2-HA were subjected to H2A.Z-IP. Inputs and IP samples  
716 were immunoblotted for H2A.Z and HA. Nab2-HA enrichment in H2A.Z pulldowns is  
717 calculated as HA/H2A.Z IP ratio, corrected for the relative Nab2-HA abundance in the input  
718 samples. Nab2-HA enrichment in WT is set arbitrarily to 1.0. All analysis was conducted  
719 from the same SDS-page gel.

Extended Data Fig. 1



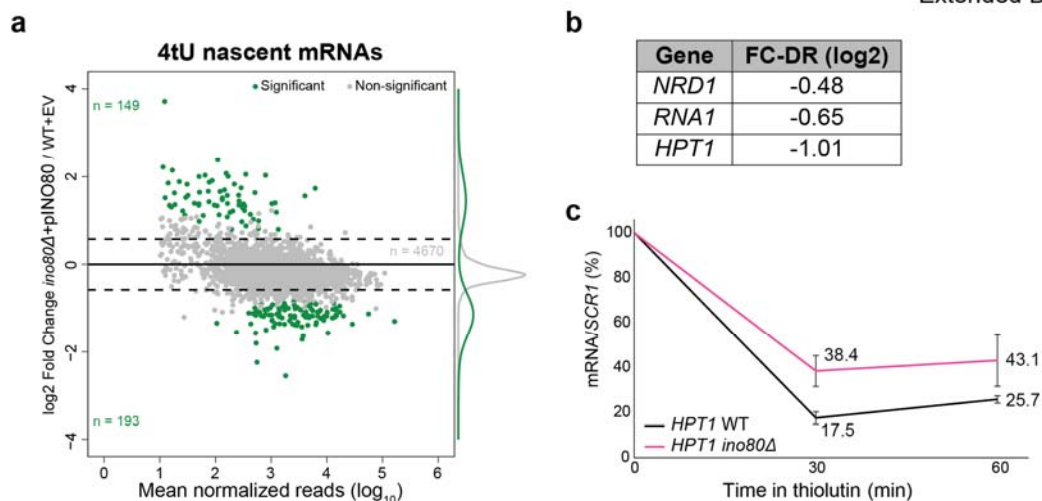
720

721 **Extended Data Fig. 1. NET-seq and 6-AU cell growth analysis in the absence of INO80.**

722 **a**, Heatmap of Pearson's correlation coefficients (R) for all pairwise combinations of NET-  
 723 seq reads in independent biological replicates. **b**, Rpb1-FLAG is efficiently  
 724 immunoprecipitated from yeast cells during NET-seq analysis. Lysates from WT and *ino80Δ*  
 725 cells expressing *RPB1-FLAG* were subjected to FLAG immunoprecipitation using FLAG  
 726 beads. Rpb1-FLAG was subsequently eluted from the beads with FLAG peptide. Input,

727 eluate and unbound samples were immunoblotted against FLAG epitope and total Rpb1.  
728 Immunoblotting against Pgk1 serves as loading control. All samples were resolved in the  
729 same SDS-page gel. **c**, Scatterplot analysis comparing the changes in NET-seq densities  
730 between WT and *ino80Δ* for sense transcripts and their relative antisense transcripts over  
731 mRNA gene regions, plotted on a log<sub>2</sub> scale. Pearson's correlation coefficient (r) is indicated.  
732 **d**, Cell proliferation analysis for the indicated strains grown exponentially in SC-ura (top  
733 panel) and in SC-ura containing 50μg/ml 6-azauracil (6-AU) (bottom panel) liquid media for  
734 the indicated time. Cell density was measured at OD<sup>620</sup> and shown on a log<sub>2</sub> scale. Shading  
735 surrounding each line denotes standard error from four independent experiments. The mutant  
736 strain deleted for the RNA Polymerase II subunit Rpb9 (*rpb9Δ*) has reported transcriptional  
737 elongation defects in 6-AU<sup>79</sup> and was used as control. Doubling time from OD<sup>620</sup> 0.2 to  
738 OD<sup>620</sup> 0.4 was calculated for all strains in both conditions. Fold Change ratio (FC) of  
739 doubling time in 6-AU over SC-ura is shown (bottom panel). **e**, 5-fold serial dilution of cells  
740 from the indicated strains were plated onto both SC-ura and SC-ura + 50μg/ml 6-Azaauracil  
741 (6-AU) and incubated at 30°C for 4-5 days. Genetic backgrounds (LS20, W303) are  
742 indicated. The mutant strain deleted for the Dst1/TFIIS transcription elongation factor (*dst1Δ*)  
743 was used as control<sup>80</sup>.

Extended Data Fig.3

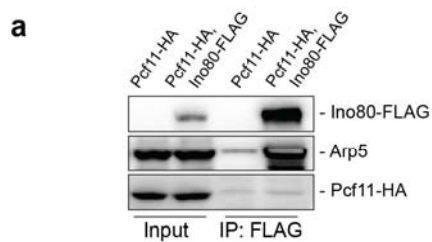


744

745

746 **Extended Data Fig. 3. Ectopic expression of INO80 rescues the nascent mRNA synthesis**  
747 **defect of *ino80*Δ cells.**

748 **a**, Scatterplot analysis for fold changes in newly synthesized mRNA between *ino80*Δ cells  
749 expressing a WT allele of *INO80* from the pRS416 plasmid (*pINO80*) and WT cells  
750 transformed with the empty vector pRS416 (EV) plotted on a log<sub>2</sub> scale. Analysis as in  
751 Fig.3a. **b**, Fold changes in mRNA decay rates between *ino80*Δ and WT for the indicated  
752 genes as calculated by cDTA analysis. **c**, RT-qPCR analysis for *HPT1* RNA was conducted  
753 in WT and *ino80*Δ before (T<sub>0</sub>) and after addition of thiolutin in YPD as in Fig. 3d.



Extended Data Fig.4

754

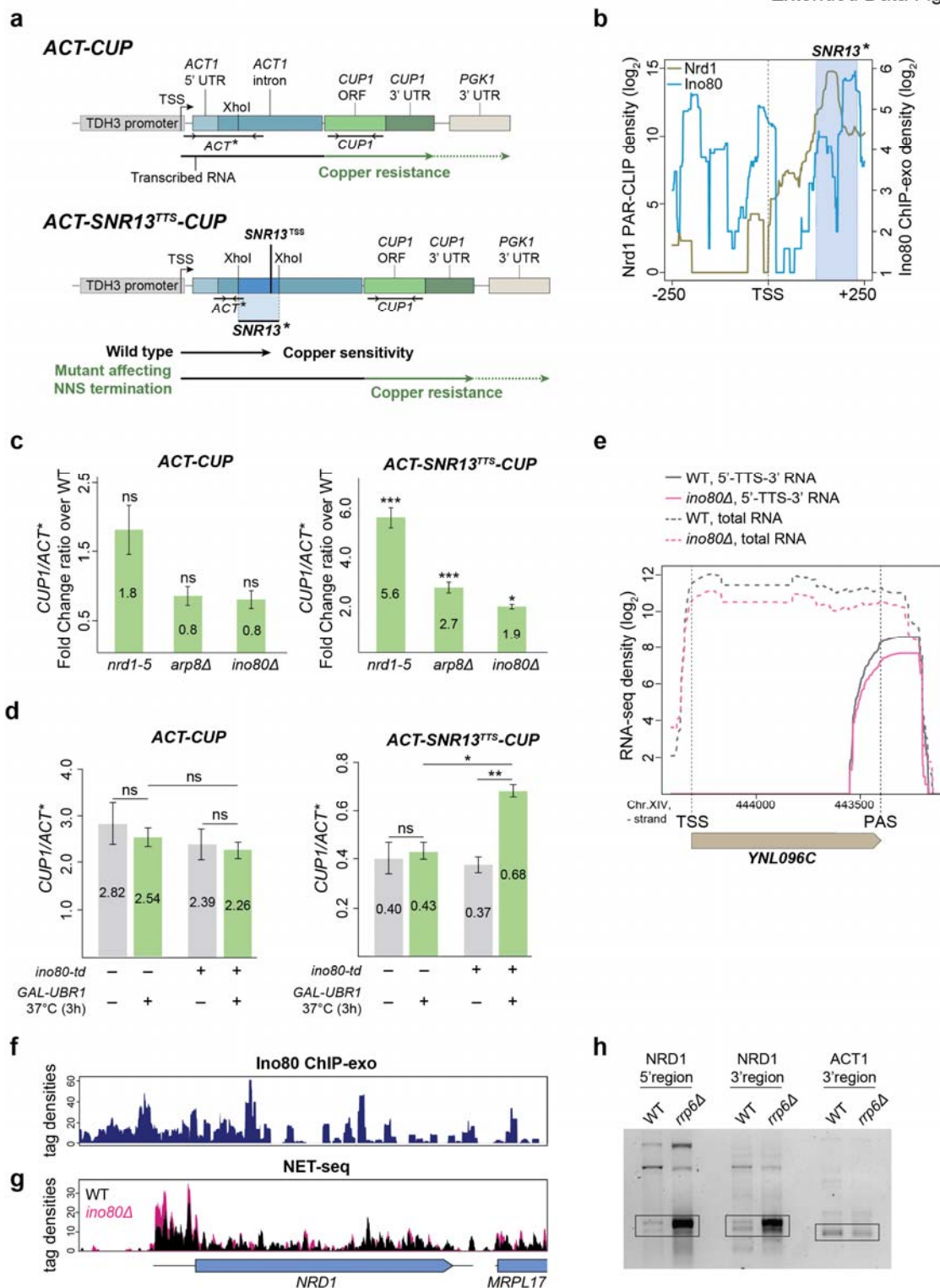
755 **Extended Data Fig. 4. INO80 does not interact with Pcf11.**

756 **a**, Nucleic acid-free lysates from cells co-expressing Pcf11-HA with Ino80 either untagged or

757 tagged with FLAG epitope were subjected to FLAG-IP. Inputs and IP samples were

758 immunoblotted for FLAG, Arp5 and HA. Samples were resolved in the same SDS-page gel.

Extended Data Fig.5



759

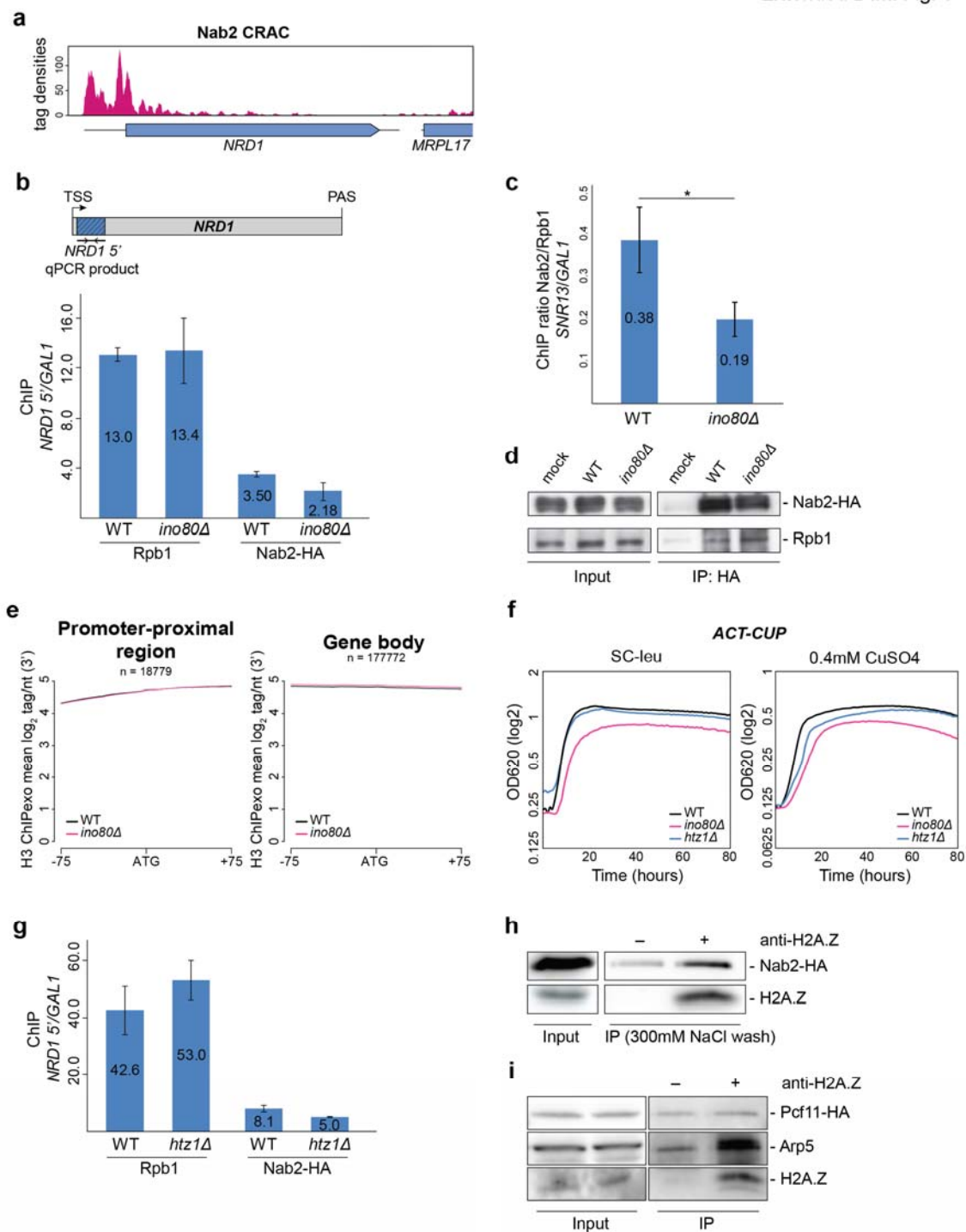
760

761 **Extended Data Fig. 5. Defective NNS-dependent transcription termination in *ino80Δ***  
762 **cells.**

763 **a**, Schematic representation of the *ACT-CUP* (pGAC24) and *ACT-SNR<sup>TTS</sup>-CUP* (pGAC24-  
764 *SNR13<sup>TTS</sup>*) reporter systems for transcription termination reported in<sup>8</sup>. The regions amplified  
765 by RT-qPCR for *ACT\** and *CUP1* are underlined. The region of the *SNR13* gene between  
766 +125 to +232bp from TSS that was cloned in the *ACT-SNR13<sup>TTS</sup>-CUP* plasmid<sup>8</sup> is shaded in  
767 blue (*SNR13\**). The expected phenotype of cells transformed with either the *ACT-CUP* or the  
768 *ACT-SNR13<sup>TTS</sup>-CUP* plasmid is shown. **b**, Snapshot of Nrd1 PAR-CLIP density profile  
769 from<sup>81</sup> and Ino80 ChIP-exo density profile from<sup>33</sup> across the *SNR13* snoRNA gene. Tags  
770 were aligned relative to TSS and plotted on a log<sub>2</sub> scale. The region between +125 to +232bp  
771 from TSS cloned in the *ACT-SNR13<sup>TTS</sup>-CUP* plasmid described in (a)<sup>8</sup> is highlighted in blue  
772 (*SNR13\**). **c**, RT-qPCR analysis for the *CUP1/ACT\** ratio was conducted in the indicated  
773 strains transformed with either the *ACT-CUP* (left panel) or *ACT-SNR<sup>TTS</sup>-CUP* (right panel)  
774 plasmids. Bars, standard errors from three independent experiments. Asterisks indicate  
775 statistical significance of the change in the respective mutant compared to the WT as  
776 calculated by t-test. ns: non-significant. \*, p<0.05. \*\*\*, p<0.001. **d**, RT-qPCR analysis was  
777 conducted in both WT and the *ino80-td* degenon-inducible strain (*ino80-td*)<sup>82</sup> transformed  
778 with the *ACT-CUP* control plasmid described in a. Galactose-induced activation for 3 hours  
779 at 37°C (+) and glucose-induced suppression (–) of the *UBR1* N-recognin in the two strains is  
780 indicated. Bars, standard errors from four independent experiments. p-values were calculated  
781 by t-test after testing for normal distribution by Shapiro-Wilk test. ns, non-significant. **e**,  
782 Snapshot representing RNA-seq densities in WT and *ino80Δ* across the ribosomal protein  
783 coding gene YNL096C. Solid lines, density of reads encompassing the transcription  
784 termination site (5'-TTS-3') as described in Fig. 6c. Analysis was performed around the  
785 polyadenylation site (PAS). Broken lines, total RNA-seq density. Genomic coordinates of

786 Chromosome XVI around the *YNL096C* gene are shown. The closest gene downstream of  
787 *YNL096C* is the *PHO23* mRNA gene (TSS: Chromosome XIV, 442509). **f**, Snapshot  
788 representing ChIP-exo densities of Ino80 from <sup>41</sup> across the *NRDI* gene. **g**, Snapshot  
789 representing NET-seq densities in WT and *ino80Δ* across the *NRDI* gene. **h**, Representative  
790 image of nested 3'RACE analysis of termination events at the *NRDI* 5' and 3' regions  
791 according to the scheme in Figure 6e and at the 3' of *ACT1* gene in WT and *rrp6Δ* on an  
792 agarose gel. Boxes indicate the most frequent termination sites. Ladder is 100bp. *ACT1*  
793 serves as loading control.

Extended Data Fig. 6



794

795 **Extended Data Fig. 6. Co-transcriptional recruitment of Nab2 to chromatin depends on**  
 796 **INO80 and H2A.Z.**

797 **a**, Snapshot representing CRAC densities for Nab2 from <sup>4</sup> across the *NRD1* gene. **b**,

798 Chromatin immunoprecipitation for Rpb1 and Nab2-HA in WT and *ino80Δ* cells. Fold

799 enrichment analysis at the promoter-proximal region of *NRD1* gene (*NRD1* 5') (upper panel,  
800 shaded in dark blue) was conducted as Fig. 7a. **c**, Chromatin immunoprecipitation for Nab2-  
801 HA and Rpb1 in WT and *ino80Δ* cells. Fold enrichment of each protein at the TTS region of  
802 *SNR13* gene was calculated relative to the *GALI* promoter after correction for input DNA  
803 levels. ChIP ratio at the TTS region of *SNR13* gene was calculated as Fold enrichment of  
804 Nab2-HA over Fold enrichment of Rpb1. Bars, standard errors from four independent  
805 experiments. p-values were calculated by t-test after testing for normal distribution by  
806 Shapiro-Wilk test. \*, p<0.05. **d**, Nucleic acid-free lysates from WT and *ino80Δ* cells both  
807 expressing Nab2-HA were subjected to HA-IP. Inputs and IP samples were immunoblotted  
808 for Rpb1 and HA. Mock, WT protein lysate subjected to immunoprecipitation with a control  
809 IgG antibody. **e**, Metagene analysis for ChIP-exo density profiles of histone H3 in WT and  
810 *ino80Δ* aligned at the A nucleotide of the ATG sites in the TSS to TSS+200bp (Promoter-  
811 proximal) and the TSS+200 to PAS (Gene body) regions. n=Number of ATG sites in each  
812 region. **f**, Cell proliferation analysis for the indicated strains transformed with the *ACT-CUP*  
813 plasmid grown exponentially in SC-ura (left panel) and in SC-ura liquid media containing  
814 0.4mM CuSO<sub>4</sub> (6-AU) (right panel) for the indicated time. Cell density was measured at  
815 OD<sup>620</sup> and is shown on a log<sub>2</sub> scale. **g**, Chromatin immunoprecipitation for Rpb1 and Nab2-  
816 HA in WT and *htz1Δ* cells. Fold enrichment analysis at the promoter-proximal region of  
817 *NRD1* gene (*NRD1* 5') was conducted as Fig. 7a. **h**, Nucleic acid-free lysates from WT cells  
818 expressing Nab2-HA were subjected to immunoprecipitation with either an anti-H2A.Z  
819 antibody (+) or a non-specific IgG antibody as a control (-), then washed in the presence of  
820 300mM NaCl. Inputs and IP samples were immunoblotted for HA and H2A.Z. All analysis  
821 was conducted from the same SDS-page gel. **i**, Nucleic acid-free lysates from cells  
822 expressing Pcf11-HA were subjected to immunoprecipitation with either an anti-H2A.Z  
823 antibody (+) or a non-specific IgG antibody as a control (-). Inputs and IP samples were

824 immunoblotted for HA, Arp5 and H2A.Z. The western for Pcf11-HA was over-exposed in  
825 order to detect the background levels of Pcf11 binding to the beads. All analysis was  
826 conducted from the same SDS-page gel.

827

828 **Extended Data Table 1 - Yeast strains used in this study**

<b>Name</b>	<b>Genotype</b>	<b>Source</b>
YM50	LS20 [ <i>Mat</i> $\Delta$ <i>ade2 can1r cyh2r lys S URA3-52 trp1</i> $\Delta$ <i>his3-<math>\Delta</math>200GAL:HO leu 2</i> $\Delta$ ]	Sandell & Zakian, <i>Cell</i> 1993
YM85	LS20 <i>ino80</i> $\Delta$ :: <i>KANMX</i>	Papamichos-Chronakis & Peterson, <i>Nat Struct Mol Biol</i> 2008
YM133	W303 <i>ubr1</i> $\Delta$ :: <i>HIS3-GAL-Myc-UBR1</i>	Jónsson <i>et al.</i> , <i>Mol Cell</i> 2004
YM135	W303 <i>ubr1</i> $\Delta$ :: <i>HIS3-GAL-Myc-UBR1 ino80</i> $\Delta$ :: <i>URA3-HA-ino80-td</i>	Jónsson <i>et al.</i> , <i>Mol Cell</i> 2004
YM143	LS20 <i>htz1</i> $\Delta$ :: <i>hisG-ura3</i> $\Delta$	Papamichos-Chronakis <i>et al.</i> , <i>Cell</i> 2011
YM181	LS20 <i>arp8</i> $\Delta$ :: <i>KANMX</i>	Papamichos-Chronakis <i>et al.</i> , <i>Cell</i> 2011
YM198	LS20 <i>hda1</i> $\Delta$ :: <i>HPHMX</i>	This study
YM199	LS20 <i>arp8</i> $\Delta$ :: <i>KANMX hda1</i> $\Delta$ :: <i>HPHMX</i>	This study
YM311	W303 [ <i>MATa ade2-1 can1-100 his3-11 leu2,3,112 trp1-1 ura3-1</i> ]	Verma <i>et al.</i> , <i>Mol Cell</i> 2011
YM334	W303 <i>arp8</i> $\Delta$ :: <i>KANMX</i>	Lafon <i>et al.</i> , <i>Mol Cell</i> 2015
YM467	LS20 <i>dst1</i> $\Delta$ :: <i>KANMX</i>	This study
YM468	LS20 <i>rpb9</i> $\Delta$ :: <i>KANMX</i>	This study
YM498	LS20 <i>rco1</i> $\Delta$ :: <i>HPHMX</i>	This study
YM499	LS20 <i>arp8</i> $\Delta$ :: <i>KANMX rco1</i> $\Delta$ :: <i>HPHMX</i>	This study
YM753	BY4741 [ <i>MATa his3<math>\Delta</math>1 leu2<math>\Delta</math>0 met15<math>\Delta</math>0 ura3<math>\Delta</math>0</i> ] <i>NRD1-3XHA::HIS3</i>	This study
YM801	46a [ <i>MATa ura3 his3 trp1 lys2 ade2 leu2 cup1</i> $\Delta$ ]	Steinmetz & Brow, <i>Mol Cell Biol</i> 1996
YM802	46a <i>nrd1-5</i>	Steinmetz & Brow, <i>Mol Cell Biol</i> 1996
YM838	LS20 <i>arp5</i> $\Delta$ :: <i>KANMX</i>	This study
YM850	BY4741 <i>PCF11-3XHA::HIS3</i>	This study
YM885	LS20 <i>RPB1-3XFLAG::KANMX</i>	This study

YM900	BY4741 <i>PCF11-3XHA::HIS3</i> <i>INO80-5XFLAG::NATMX</i>	This study
YM901	BY4741 <i>NRD1-3XHA::HIS3 INO80-5XFLAG::NATMX</i>	This study
YM903	LS20 <i>RPB1-3XFLAG::KANMX ino80Δ::HPHMX</i>	This study
YM1002	46a <i>arp8Δ::HPHMX</i>	This study
YM1036	46a <i>nrd1-5 arp8Δ::HPHMX</i>	This study
YM1085	LS20 <i>xrn1Δ::KANMX</i>	This study
YM1139	LS20 <i>rrp6Δ::KANMX</i>	This study
YM1141	46a <i>rco1Δ::KANMX</i>	This study
YM1147	46a <i>nrd1-5 arp8Δ::HPHMX rco1Δ::KANMX</i>	This study
YM1197	BY4741 <i>abd1-DAmP::KANMX</i>	Breslow <i>et al</i> , <i>Nat Methods</i> 2008
YM1325	LS20 <i>NAB2-3XHA::KANMX</i>	This study
YM1331	LS20 <i>NAB2-3XHA::KANMX ino80Δ::HPHMX</i>	This study
YM1332	LS20 <i>NAB2-3XHA::KANMX ino80Δ::HPHMX</i>	This study
YM1452	LS20 <i>NAB2-3XHA::KANMX htz1Δ::HPHMX</i>	This study

830 **Extended Data Table 2 – Expression of genes encoding for RNA surveillance proteins is**  
 831 **similar in WT, *ino80Δ* and *arp8Δ* cells.** RNA abundance for the listed genes was measured  
 832 by spiked-in total RNA-seq analysis in the indicated strains. Values represent average from  
 833 two biological replicates for each experiment. The RNA-seq experiment for WT<sup>(1)</sup> and  
 834 *ino80Δ* was conducted independently from WT<sup>(2)</sup> and *arp8Δ*. Values represent average from  
 835 two biological replicates for each experiment.

<b>Pathway/complex</b>	<b>Gene</b>	<b>WT<sup>(1)</sup></b>	<b><i>ino80Δ</i></b>	<b>Fold Change</b>	<b>WT<sup>(2)</sup></b>	<b><i>arp8Δ</i></b>	<b>Fold Change</b>
<b><i>NNS</i></b>	<i>NRD1</i>	0.61	0.67	<b>1.1</b>	0.43	0.37	<b>0.8</b>
	<i>NAB3</i>	0.54	0.44	<b>0.8</b>	0.30	0.30	<b>1.0</b>
	<i>SEN1</i>	0.46	0.58	<b>1.3</b>	0.29	0.25	<b>0.8</b>
<b><i>Exosome</i></b>	<i>RRP6</i>	0.68	0.54	<b>0.8</b>	0.46	0.46	<b>1.0</b>
	<i>DIS3/RRP44</i>	0.82	0.73	<b>0.9</b>	0.64	0.62	<b>1.0</b>
<b><i>TRAMP</i></b>	<i>MTR4</i>	0.97	0.74	<b>0.8</b>	0.87	0.89	<b>1.0</b>
	<i>TRF4</i>	0.45	0.48	<b>1.1</b>	0.28	0.32	<b>1.1</b>
	<i>AIR1</i>	0.38	0.30	<b>0.8</b>	0.29	0.29	<b>1.0</b>
	<i>AIR2</i>	0.21	0.22	<b>1.1</b>	0.11	0.15	<b>1.4</b>
<b><i>Cleavage and Polyadenylation</i></b>	<i>HRP1</i>	1.21	1.01	<b>0.8</b>	1.04	0.83	<b>0.8</b>
	<i>PCF11</i>	0.26	0.24	<b>0.9</b>	0.19	0.18	<b>1.0</b>
	<i>NAB2</i>	0.70	0.59	<b>0.8</b>	0.51	0.54	<b>1.1</b>
	<i>PAB1</i>	8.95	6.85	<b>0.8</b>	4.53	3.89	<b>0.9</b>
<b><i>Capping</i></b>	<i>CEG1</i>	0.42	0.44	<b>1.1</b>	0.19	0.22	<b>1.1</b>
	<i>CET1</i>	0.27	0.26	<b>1.0</b>	0.17	0.19	<b>1.1</b>
<b><i>Early mRNA processing</i></b>	<i>CBC1</i>	0.96	0.74	<b>0.8</b>	0.58	0.68	<b>1.2</b>
	<i>GBP2</i>	1.43	1.09	<b>0.8</b>	0.83	0.74	<b>0.9</b>
	<i>THO2</i>	0.48	0.51	<b>1.0</b>	0.27	0.31	<b>1.2</b>
<b><i>Export</i></b>	<i>MEX67</i>	0.52	0.50	<b>1.0</b>	0.32	0.34	<b>1.1</b>
<b><i>Cytoplasmic decay</i></b>	<i>XRN1</i>	1.87	1.76	<b>0.9</b>	0.91	0.91	<b>1.0</b>
	<i>SKI2</i>	0.40	0.40	<b>1.0</b>	0.28	0.31	<b>1.1</b>

836

837 **Extended Data Table 3 – Readthrough index (RI) of budding yeast *SNR* snoRNA genes**  
838 **as measured by total RNA-seq from the indicated strains.** The RNA-seq experiment for  
839 WT<sup>(1)</sup> and *ino80Δ* was conducted independently from WT<sup>(2)</sup>, *xrn1Δ*, *rrp6Δ*. Values represent  
840 average from two biological replicates for each experiment.

	WT <sup>(1)</sup>	<i>ino80Δ</i>	WT <sup>(2)</sup>	<i>xrn1Δ</i>	<i>rrp6Δ</i>
<i>NME1</i>	0.05	0.10	0.09	0.12	0.06
<i>SNR11</i>	0.18	0.17	0.26	0.23	0.24
<i>SNR128</i>	0.29	0.36	0.36	0.38	0.29
<i>SNR13</i>	0.15	0.28	0.44	0.36	0.25
<i>SNR161</i>	0.20	0.21	0.30	0.20	0.15
<i>SNR189</i>	0.22	0.23	0.47	0.39	0.33
<i>SNR190</i>	0.01	0.01	0.01	0.01	0.01
<i>SNR3</i>	0.90	1.05	0.91	0.87	0.68
<i>SNR30</i>	0.11	0.16	0.25	0.24	0.51
<i>SNR31</i>	0.18	0.15	0.17	0.17	0.13
<i>SNR32</i>	0.64	0.63	0.73	0.83	0.67
<i>SNR33</i>	0.41	0.39	0.47	0.37	0.51
<i>SNR34</i>	0.49	0.55	0.55	0.41	0.29
<i>SNR35</i>	0.17	0.20	0.27	0.17	0.17
<i>SNR36</i>	0.36	0.38	0.33	0.29	0.25
<i>SNR37</i>	0.32	0.37	0.46	0.42	0.72
<i>SNR39B</i>	0.41	0.57	0.50	0.41	0.93
<i>SNR4</i>	0.17	0.18	0.18	0.15	0.34
<i>SNR40</i>	0.61	0.70	0.62	0.70	0.53
<i>SNR41</i>	0.23	0.22	0.22	0.31	0.34
<i>SNR42</i>	0.42	0.37	0.98	0.59	0.95
<i>SNR43</i>	0.23	0.24	0.35	0.40	0.73
<i>SNR45</i>	1.15	1.04	0.99	0.84	1.57
<i>SNR46</i>	0.37	0.58	0.52	1.06	0.20
<i>SNR47</i>	0.56	1.21	0.52	0.56	1.61
<i>SNR48</i>	0.59	0.71	0.75	0.76	0.93
<i>SNR49</i>	0.53	0.62	0.43	0.41	0.21
<i>SNR5</i>	0.42	0.44	0.53	0.45	0.57
<i>SNR50</i>	1.30	1.08	1.00	0.97	1.76
<i>SNR51</i>	0.79	1.30	1.03	0.76	1.45
<i>SNR52</i>	0.47	0.51	0.52	0.42	0.60
<i>SNR53</i>	0.54	0.79	0.52	0.65	0.74
<i>SNR55</i>	0.39	0.57	0.42	0.55	0.28
<i>SNR56</i>	0.40	0.68	0.46	0.52	2.72
<i>SNR57</i>	0.66	0.64	0.60	0.62	0.71
<i>SNR58</i>	1.01	0.87	1.14	0.69	1.07

<b>SNR61</b>	1.57	2.83	1.19	0.85	2.76
<b>SNR62</b>	1.78	2.03	1.66	1.51	3.55
<b>SNR63</b>	0.40	0.52	0.66	0.43	0.55
<b>SNR64</b>	0.33	0.49	0.22	0.23	0.49
<b>SNR65</b>	0.74	0.95	1.09	0.30	3.17
<b>SNR66</b>	1.23	2.42	1.07	1.33	1.74
<b>SNR67</b>	1.07	1.01	1.08	1.14	1.44
<b>SNR68</b>	0.36	0.75	0.82	0.60	1.09
<b>SNR69</b>	0.68	0.88	0.75	0.80	0.70
<b>SNR70</b>	1.56	1.72	2.16	2.34	1.28
<b>SNR71</b>	1.38	2.61	1.41	1.39	3.46
<b>SNR72</b>	0.39	0.62	0.33	0.37	0.42
<b>SNR74</b>	1.10	1.29	1.05	1.53	0.47
<b>SNR75</b>	2.10	2.46	1.72	2.14	1.37
<b>SNR76</b>	0.57	0.52	0.46	0.44	0.30
<b>SNR77</b>	1.07	1.27	1.07	1.13	0.62
<b>SNR78</b>	3.67	4.40	4.26	5.35	4.26
<b>SNR79</b>	1.73	1.63	1.65	1.23	2.45
<b>SNR8</b>	0.27	0.27	0.21	0.22	0.27
<b>SNR80</b>	0.06	0.17	0.14	0.13	0.23
<b>SNR81</b>	0.15	0.28	0.23	0.19	0.12
<b>SNR82</b>	0.66	0.77	0.92	0.89	0.94
<b>SNR83</b>	0.35	0.46	0.46	0.30	1.03
<b>SNR84</b>	0.58	0.77	0.60	0.81	0.26
<b>SNR85</b>	0.02	0.02	0.03	0.02	0.08
<b>SNR86</b>	0.41	0.40	0.25	0.26	0.17
<b>SNR87</b>	0.93	1.16	1.04	0.90	1.38
<b>SNR9</b>	0.28	0.32	0.38	0.36	0.27

## 842 **METHODS**

### 843 **Bioinformatics Tools and genome annotations**

844 Unless otherwise indicated, version of the tools used for all bioinformatics analyses are as  
845 follows:

846 Samtools version 1.10

847 Bedtools version 2.29.2

848 Bowtie2 version 2.4.1

849 Hisat2 version 2.2.0

850 R version 3.6.2

851 BamCoverage version 3.5.0

852 Fastqc version 0.11.9

853 Cutadapt version 2.10

854 Trim\_galore 0.6.4

855 MarkDuplicates version 2.23.1

856 FeatureCounts version 2.0.0

857 The *Saccharomyces cerevisiae* reference genome (S288C version R64-2-1) was downloaded  
858 from Saccharomyces Genome Database (<https://www.yeastgenome.org/>). The annotation  
859 used in the analysis for mRNA genes was produced by Antonin Morillon's lab, and based on  
860 CAGE-seq. This also includes the following annotations: XUT genes from <sup>83</sup>, SUT and CUT  
861 genes from XUT et al (2009) and NUT genes from <sup>16</sup>. Annotations for other transcript types  
862 (snRNA, snoRNA, etc) were downloaded from Saccharomyces Genome Database.

863 The *Schizosaccharomyces pombe* reference genome and annotation (ASM294v2.47) were  
864 downloaded from pombase ([www.pombase.org](http://www.pombase.org)). Only protein coding genes were used in this  
865 analysis.

### 866 **NET-seq analyses**

867 NET-seq was performed from yeast strains containing Rpb1-FLAG (3XFLAG), alone or  
868 along with deletion of *INO80*. All strains appeared fully functional, with identical Ser2 and  
869 Ser5 phosphorylation levels on Rpb1 C-terminal domain and identical growth rates to the  
870 respective untagged strains (data not shown). NET-Seq libraries were constructed from  
871 biological duplicates of YM903 (*ino80Δ*, *RPB1-FLAG*) and YM885 (WT, *RPB1-FLAG*) cells  
872 and sequenced as previously described<sup>84</sup>. Reads shorter than 10 nt were filtered out. Reads  
873 were mapped with Bowtie2 using default parameters. Duplicates reads were marked using  
874 Picard MarkDuplicates. Coverage files (bigWig) were produced by custom script. Reads  
875 locations from the alignment files (bam) were turned into bed files using bedtools bamtobed  
876 (with « -split » option), ignoring duplicates reads and reads with mapping quality below 30,  
877 piled up along the genome and turned into bigWig files using a python script. FeatureCounts  
878 was used for quantification with options « -O --fraction s 2 --ignoreDup ». Normalization  
879 factors were computed using DESeq2 method, using the whole count matrix. Travelling  
880 Ratio was computed as: (read density on gene body) / (read density on TSS), with gene body  
881 the region between TSS+200 nt to TTS and TSS the region from TSS to TSS + 200 nt. Read  
882 density was computed as : (# reads on region / region length) \*1000.

### 883 **4tU labeling and purification of newly synthesized RNAs**

884 RNA labeling and purification were performed as previously described with some minor  
885 adjustments<sup>45,85</sup>. Briefly, 20 mL of wildtype and mutant *S. cerevisiae* cells were grown at  
886 30°C to an OD600 ≈0.8 in YPD. Newly synthesized (ns) RNAs were labelled for 6 min with  
887 4-thiouracil (4tU, Sigma-Aldrich) added to the yeast cultures to a final concentration of 5  
888 mM. Similarly, *S. pombe* RNAs were labeled for 6 min in YES medium at 32°C. Cells were  
889 pelleted directly after labeling and flash frozen in liquid nitrogen. All experiments were  
890 performed in biological triplicates. Prior to RNA extraction *S. cerevisiae* and *S. pombe* cells  
891 were mixed in a ratio of 3:1 and total RNA was extracted with Ribopure Yeast Kit (Ambion,

892 Life Technologies) according to the manufacturer's guidelines. 150  $\mu$ g of total RNA were  
893 biotinylated for 3 hours at room temperature using 200  $\mu$ L of 1 mg/mL EZ-link HPDP-  
894 Biotin (Pierce) with 100  $\mu$ L of biotinylation buffer (100 mM Tris- HCl pH 7.5, 10 mM  
895 EDTA) and 100  $\mu$ L of DMSO adjusted to a final volume of 1 mL with DEPC-treated RNase-  
896 free water (Sigma-Aldrich). After biotinylation, excess biotin was removed by mixing 1 mL  
897 of chloroform to the reaction and the liquid phases were separated by centrifugation for 5 min  
898 at 4°C and max speed. The aqueous phase was recovered and precipitated with isopropanol  
899 (1/10 volumes 5M NaCl and 2.5 volumes isopropanol). The recovered RNA was resuspended  
900 in 100  $\mu$ L DEPC-treated RNase-free water and incubated for 10 min at 65°C followed by 5  
901 min on ice. nsRNAs were bound to 100  $\mu$ L of  $\mu$ MACS streptavidin microbeads (Miltenyi  
902 Biotec) for 90 min at room temperature and purification was performed using the  $\mu$ MACS  
903 streptavidin starting kit (Miltenyi Biotec). Columns were first equilibrated with 1 mL of  
904 washing buffer (100 mM Tris-HCl at pH 7.5, 10 mM EDTA, 1M NaCl, 0.1% Tween20).  
905 Samples were loaded and the flow-through was reapplied 2 times to the columns. The  
906 columns were washed five times with increasing volumes of washing buffer (600, 700, 800,  
907 900, and 1000  $\mu$ L). Ultimately, labeled RNAs were eluted twice with 200  $\mu$ L of 100mM  
908 DTT. nsRNAs were precipitated overnight in 1/10 volume of 3 M NaOAc, 3 volumes of  
909 100% ethanol and 20  $\mu$ g of RNA-grade glycogen. The RNAs were recovered by  
910 centrifugation and RNA pellets were wash with ice-cold 70% ethanol and resuspended in 20  
911  $\mu$ L of DEPC-treated RNase-free water (Sigma-Aldrich). Samples were stored at -80°C until  
912 further use. Differential gene expression analysis was performed using DESeq2 1.16.1  
913 Bioconductor R package on *Saccharomyces cerevisiae* counts normalized with size factors  
914 computed by the median-of-ratios method proposed by Anders and Huber on  
915 *Schizosaccharomyces pombe* counts (Anders and Huber 2010). cDTA analysis was  
916 performed as described (Schwalb et al. 2012).

917

## 918 **Total RNA-seq**

919 Yeast strains were processed in duplicate. ERCC RNA Spike-in control mixes (Ambion,  
920 catalogue #4456740) were added to 1µg of total RNA according to manufacturer. Ribosomal  
921 RNAs were depleted from total RNA using the RiboMinus™ Eukaryote v2 Kit (Life  
922 Technologies). Depletion efficiency and quality control of rRNA-depleted RNA was assessed  
923 by analysis in RNA Pico 6000 chip for 2100 Bioanalyzer (Agilent). Total RNA-seq libraries  
924 were prepared from 50ng of rRNA-depleted RNA using the TruSeq® Stranded Total RNA  
925 Sample Preparation Kit (Illumina). Paired-end sequencing (2x50 nt) was performed on a  
926 HiSeq 2500 sequencer giving between 65 and 84 million reads. Reads were mapped using  
927 version 2.0.6 of TopHat, with a tolerance of 3 mismatches and a maximum size for introns  
928 2Kb. Tags densities were normalized on spike-in controls for all subsequent analyses.

## 929 **ChIP-exo**

930 The ChIP-exo assay has been previously described (Rhee HS, Pugh BF. ChIP-exo method for  
931 identifying genomic location of DNA-binding proteins with near-single-nucleotide accuracy.  
932 Curr Protoc Mol Biol. 2012;Chapter 21:Unit 21). In brief, yeast strains were grown to  
933 exponential phase in yeast extract peptone (YP) + 2% dextrose (30°C to OD600 nm = 0.8),  
934 then subjected to 1% formaldehyde crosslinking for 15 min at 25°C. After quenched with  
935 125mM final concentration of glycine for 5 min, cells were harvested and washed. Sonicated  
936 chromatin was prepared by standard methods. Standard ChIP methods were used for histone  
937 H3 (antibody Ab1791, Abcam) followed by lambda exonuclease treatment and library  
938 construction. Libraries were sequenced on an Illumina 2000 sequencer. Reads were uniquely  
939 mapped to the reference genome (sacCer3 build) using version 2.1.0 of Bowtie2 with a  
940 tolerance of 1 mismatch in seed alignment. Data were normalized on the total number of  
941 uniquely mapped reads, for each sample.

## 942 **Cell proliferation analysis in liquid media**

943 Liquid growth rate analysis was conducted using the CG-12 robot (S&P Robotics Inc.). Yeast  
944 cells transformed with a URA3-containing plasmid (pRS416) and grown exponentially in  
945 SC-ura at 30°C were diluted to OD<sub>620</sub> 0.1 in either SC-ura or SC-ura + 50µg/ml 6-AU and  
946 four 150µl samples from each strain were plated onto 96-well transparent plates covered with  
947 breathable films. Plates were incubated at 30°C for several days and OD<sub>620</sub> was measured in  
948 the CG-12 robot (S&P Robotics Inc.) every hour with a shaking of 1000rpm for 1 minute  
949 before each read. Liquid growth rate analysis was not possible in the *nrđ1-5* and associated  
950 strains due to flocculation. All cell proliferation experiments were repeated at least twice.

## 951 **Growth rates analysis on agar plates**

952 Growth of yeast strains was compared by plating 5-fold serial dilutions on SC / SC-inositol,  
953 SC-ura / SC-ura + 50µg/ml 6-azauracil (6-AU, Sigma), SC-leu / SC-leu + 0.4mM CuSO<sub>4</sub>  
954 (Sigma) or SC-leu / SC-leu + 0.25 CuSO<sub>4</sub> and incubating the plates at 30°C for several days.  
955 All plating experiments were performed at least three times.

## 956 **RT-qPCR**

957 Total RNA was extracted either with RNeasy Mini Kit (Qiagen) or by classical acid phenol-  
958 chloroform extraction. RNAs abundance was measured with SuperScript® III Platinum®  
959 SYBR® Green One-Step qRT-PCR Kit (Invitrogen) using specific primers for the targets of  
960 interest in a 10µl reaction volume, on Applied Biosystem Step-One Plus machines. RNAs  
961 abundance of each sample was compared with standard curves analysis. Abundance of *CUP1*  
962 from transcriptional read-through analyses using the *ACT-CUP* reporter system was  
963 compared to *ACT\** RNA specifically transcribed from the same plasmid (Extended Data  
964 Fig.5a). Abundance of *NRĐ1* promoter-proximal RNA (*NRĐ1* 5') was compared to levels of  
965 *NRĐ1* promoter-distal RNA (*NRĐ1* 3').

## 966 **Co-immunoprecipitation**

967 Benzonase-treated yeast cell extracts were incubated with 20µl Anti-FLAG Affinity Gel  
968 (Sigma Aldrich) in 10mM Tris-Cl pH 7.5, 150mM NaCl, 0.05mM EDTA, 0.5% NP40, 1X  
969 Protease Inhibitor Cocktail (Roche) and 0.01mM PMSF for 3h. Beads were washed twice in  
970 10mM Tris-Cl pH 7.5, 150mM NaCl, 0.05mM EDTA, 1X Protease Inhibitor Cocktail  
971 (Roche) and 0.01mM PMSF and resuspended in SDS sample buffer. Western blot analyses  
972 were performed using Monoclonal anti-FLAG M2 antibody (Sigma F3165), Anti-HA tag  
973 antibody (Abcam, ab9110) and Anti-Arp5 antibody (Abcam, 12099). Images were acquired  
974 using Syngene G:BOX. The experiment was reproduced three times. Immunoprecipitations  
975 for H2A.Z and HA-tag were performed similarly on benzonase-treated yeast cell extract  
976 using 36µl Protein-A sepharose beads coupled with 6µl of appropriate antibody (Anti-  
977 H2A.Z, Active Motif 39647; Anti-HA tag, Abcam ab9110). Control immunoprecipitations  
978 (mock) were performed with a non-specific antibody (Anti-Rabbit IgG, Promega). Western  
979 blot analyses were performed using the following antibodies: Anti-HA, Anti-Arp5, Anti-  
980 H2A.Z and Anti-Rpb1 y-80 (Santa Cruz Biotechnology, sc-25758). After the  
981 immunoprecipitation for H2A.Z shown in Figure S6G, beads were washed twice in 10mM  
982 Tris-Cl pH 7.5, 150mM NaCl, 0.05mM EDTA, 1X Protease Inhibitor Cocktail (Roche) and  
983 0.01mM PMSF, then washed a third time in the same buffer containing 300mM NaCl and  
984 finally resuspended in SDS sample buffer All experiments were reproduced three times.

### 985 **Ino80 inducible degradation**

986 The assay for inducible degradation of Ino80<sup>82</sup> was performed as previously described<sup>35,86</sup>  
987 Briefly, a degron tag was fused to INO80 (Ino80-td) in cells carrying the UBR1 gene, that  
988 encodes for the N-recognin Ubr1, under the control of the GAL1 promoter, and cells were  
989 transformed with the *ACT-CUP* plasmid reporter system (Extended Data Fig. 5a). Cells were  
990 grown in SC-leu media containing raffinose as carbon source at 25°C until OD600~0.6-0.7,  
991 then shifted to SC-leu media containing galactose to induce *UBR1* expression. Subsequently,

992 complete Ino80-td protein degradation by the Ubr1 pathway was induced by 3 hours of heat  
993 shock at 37°C. Cells were then immediately harvested by centrifugation at 4°C, 3500rpm for  
994 3 minutes, then washed twice with ice-cold water and snap-frozen in liquid nitrogen for RNA  
995 analysis. Yeast cells carrying the GAL1-driven UBR1 gene along with an unmodified INO80  
996 genes were use as control. Furthermore, both (GAL1-UBR1) and (GAL1-UBR1 Ino80-td)  
997 cells were grown in SC-leu media containing glucose as a negative control for UBR1  
998 expression (Extended Data Fig. 5d, grey bars). RNA analysis was conducted by RT-qPCR as  
999 described above.

#### 1000 **ChIP-qPCR**

1001 Chromatin immunoprecipitation was performed as previously described in (Papamichos-  
1002 Chronakis M, Watanabe S, Rando OJ, Peterson CL. Global regulation of H2A.Z localization  
1003 by the INO80 chromatin-remodeling enzyme is essential for genome integrity. Cell.  
1004 2011;144(2):200-13.). Sonication was performed on a Bioruptor® Pico sonication device  
1005 (Diagenode) with ten 30-sec pulses with a 30-sec break between pulses. Immunoprecipitation  
1006 was carried out with Anti-HA tag antibody (Abcam ab9110) and Anti-Rpb1 y-80 antibody  
1007 (Santa Cruz Biotechnology, sc-25758) in parallel. The recovered DNA was subjected to  
1008 quantitative real-time PCR using Platinum® SYBR® Green qPCR SuperMix-UDG Kit  
1009 (Invitrogen) with specific primers for the targets of interest in 10µl reaction volume, on  
1010 Applied Biosystem Step-One Plus machines.

#### 1011 **RNA-IP**

1012 RNA immunoprecipitation was performed as described in (Selth LA, Gilbert C, Svejstrup JQ.  
1013 RNA immunoprecipitation to determine RNA-protein associations in vivo. Cold Spring Harb  
1014 Protoc. 2009;2009(6):pdb prot5234.). Sonication was performed on a Bioruptor® Plus  
1015 sonication device (Diagenode) with two 15-sec pulses at 50% amplitude with a 1-min break

1016 between pulses. Immunoprecipitation was carried out with Anti-HA tag antibody (Abcam  
1017 ab9110). The recovered RNA was analysed by RT-qPCR as described above.

1018 **De novo analysis of public ChIP-exo and CRAC data**

1019 NAB3 and POLII CRAC data were taken from GEO dataset GSE70191 and processed as  
1020 described in <sup>56</sup>. NAB2 and MTR CRAC data were taken from GEO dataset GSE46742 and  
1021 processed as described in <sup>4</sup>. ChIP-exo H3 data were downloaded from NCBI SRA dataset  
1022 SRA059355 and processed as described in <sup>87</sup>.